Variability of phytoplankton light absorption in stratified waters of the NW Mediterranean Sea: the interplay between pigment composition and the packaging effect

Gonzalo L. Pérez [a,*], Martí Galí [b], Sarah-Jeanne Royer [c], Marina Gerea[a], Eva Ortega-Retuerta[d,e], Josep M. Gasol[e, f], Cèlia Marrasé [e], Rafel Simó [e]

[a] GESAP (Grupo de Ecología de Sistemas Acuáticos a escala de Paisaje), Instituto de Investigaciones en Biodiversidad y Medioambiente (INIBIOMA, UNComahue-CONICET), Quintral 1250, R8400FRD, San Carlos de Bariloche, Río Negro, Argentina.

[b] Barcelona Supercomputing Center (BSC-CNS), Barcelona, Catalonia, Spain.

[c] Marine Biology Research Division, Scripps Institution of Oceanography, UC San Diego, 9500 Gilman Drive, La Jolla, CA 92093, USA

[d] CNRS, Sorbonne Université, UMR 7621, Laboratoire d'Océanographie Microbienne, Banyuls-sur-Mer, France.

[e] Institut de Ciències del Mar, CSIC, Passeig Marítim de la Barceloneta 37-49, 08003 Barcelona, Catalonia, Spain

[f] Centre for Marine Ecosystems Research, School of Sciences, Edith Cowan University, Joondalup, WA, Australia

*Corresponding author: E-mail address: gonzaloperez@comahue-conicet.gob.ar (G. L. Pérez)

Keywords: phytoplankton absorption, pigment composition, packaging effect, community size structure, photoacclimation, North-Western Mediterranean Sea

Abstract

The Variability of chlorophyll-specific phytoplankton light absorption [$a^*_{ph}(\lambda)$] was examined over depth and time in stratified offshore waters of the North-Western Mediterranean Sea. Coherent water patches were tracked with Lagrangian drifters during two oceanographic cruises in September (late summer) and May (post-spring bloom phase). By simultaneously analysing the phytoplankton absorption and pigment measurements, we explicitly separated the impact of pigment composition from that of pigment packaging on $a^*_{ph}(\lambda)$. We further partitioned the packaging effect by comparing the variation of the packaging index [$Q_a^*(440)$], the phytoplankton community size structure (derived from diagnostic pigment analysis), and the chlorophyll-specific beam attenuation by particles [$c_p^*(660)$] as an optical index of phytoplankton photophysiology. In the ensemble of cruises, around 50% of the $a^*_{ph}(440)$ vertical variation was explained by changes in the pigment composition (ruled by the decrease of photoprotective pigments with depth). The remaining vertical and inter-cruise variation of $a^*_{ph}(440)$ was attributed to the packaging effect. We found that differences in the $c_p^*(660)$ index (most likely indicating changes in the intracellular pigment concentration due to photoacclimation) mainly explained the observed variation in the packaging effect. Differences in $c_p^*(660)$ were coincident with either the vertical gradient of light availability or the lower mean daily PAR irradiance in the euphotic layer of the September cruise. These explained the stronger packaging and lower $a^*_{ph}(440)$ values observed with increasing depth in both cruises, and in September relative to May. On the other hand, differences in the phytoplankton community size structure did not explain the observed patterns in the packing effect. Our results highlight the importance of phytoplankton short-term acclimation to the prevailing light conditions, determining the vertical and temporal variability of $a^*_{ph}(\lambda)$. A better understanding of the $a^*_{ph}(\lambda)$ variability and its main drivers are key to improve different bio-optical applications.

1.0 INTRODUCTION

The absorption and scattering coefficients of various optically active constituents determine the ocean's optical properties (Preisendorfer, 1961). Among them, the *in vivo* phytoplankton spectral absorption coefficient [a_{ph} (λ), m^{-1}] is a critical component because it quantifies phytoplankton potential light absorption, providing an optical signature of the autotrophic community in the ~380-700 nm spectral region (Johnsen et al., 2011; Morel, 1978). Its chlorophyll-specific counterpart [a^*_{ph} (λ), m^2 mg^{-1}], constitutes the link between phytoplankton biomass and light absorption. Altogether, a_{ph} (λ) and a^*_{ph} (λ) are key to understand the quantitative regional and global significance of phytoplankton to ocean ecology and biogeochemical cycling.

Characterization of a_{ph} (λ), as well as the drivers of its natural variability, is essential for a variety of research applications, including the study of light propagation and ocean thermal structure (Chang and Dickey, 2004; Sathyendranath and Platt, 1988), algal physiology (Moore et al., 1995; Morel et al., 1993; van Leeuwe et al., 2005) and modelling of primary production (PP) (Marra et al., 2007; Morel et al., 1996). Furthermore, since a_{ph} (λ) affects the ocean spectral reflectance, it is important for ocean colour remote sensing applications such as the retrieval of *chlorophyll a* (*Chl a*) (D'Ortenzio et al., 2002; O'Reilly et al., 1998; Siegel et al., 2013; Volpe et al., 2007), the estimation of PP (Behrenfeld and Falkowski, 1997; Lee et al., 2015; Morel, 1991; Tilstone et al., 2015) and the inference of phytoplankton size, functional types and taxonomic composition (Brewin et al., 2011; Bricaud et al., 2012; Zeng et al., 2018).

The variability of a_{ph} (λ) at different spatial and temporal scales has been widely studied over the past 25 years in regions of the world's oceans. Studies have shown that the variability of a_{ph} (λ) magnitude is mainly explained by differences in *Chl a* concentration (as a proxy of phytoplankton biomass). In spite of the strong covariation between a_{ph} (λ) and *Chl a*, a^*_{ph} (λ) is generally far from being constant because it is affected by pigment composition and by the pigment packaging effect (Bricaud et al., 1999, 1995; Cleveland, 1995; Mitchell and Kiefer, 1988). This latter effect is defined as the reduction in the absorption of pigmented particles relative to the absorption of the pigments in solution. It is predicted by theory to depend on phytoplankton size and intracellular pigment concentrations. As a consequence, the packaging effect increases with cell size and cellular pigment content; as a consequence, higher values of a^*_{ph} (λ) are expected for small cells with low intracellular pigment concentrations (Kirk, 1976; Morel and Bricaud, 1981).

In natural waters, the effects of the different causes that contribute to the variability of a^*_{ph} (λ) are intermingled and are commonly difficult to evaluate individually. Various methods have been implemented to explicitly separate the influences of pigment composition and packaging effect (see, e.g., Bricaud et al., 2004; Lohrenz et al., 2003; Stæhr et al., 2004; Stuart et al., 1998). Different approaches have also been proposed to independently quantify the impact of the algal community size structure on pigment packaging (Bricaud et al., 2004a; Ferreira et al., 2009). Diagnostic accessory pigments analysis (DPA) has been used to estimate the relative proportions of the three phytoplankton size classes (micro-, nano- and picophytoplankton) (Uitz et al., 2006; Vidussi et al., 2001). From DPA, a size index (*SI*) was derived to obtain a single indicator of the average size of

the phytoplankton population within the first optical depth (Bricaud et al., 2004). This has been frequently used to relate changes in phytoplankton cell size with the variability of $a^*_{ph}(\lambda)$ (e.g., Bricaud et al., 2010; Nunes et al., 2019; Wang et al., 2014). Instead, also for surface layers, Ciotti et al. (2002) proposed the use of the spectral shape of $a_{ph}(\lambda)$ to determine the cell size factor (S_f), being this procedure also used to explain $a^*_{ph}(\lambda)$ variability (Ferreira et al., 2013, 2017; Kheireddine et al., 2018a).

The relative contributions of the different factors affecting $a^*_{ph}(\lambda)$ depend on the spatial dimension under analysis. In horizontal surveys across surface waters, the dominant source of $a^*_{ph}(\lambda)$ variability generally results from differences in the pigment packaging due to changes in the size structure of phytoplankton populations (e.g., Bricaud et al., 2004; Ciotti et al., 2002; Ferreira et al., 2013). In contrast, in the vertical dimension of oligotrophic stratified waters, the variability of $a^*_{ph}(\lambda)$ is mainly related to gradients of photoprotective carotenoids and changes in the intracellular pigment concentration resulting from photoacclimation (e.g., Allali et al., 1997; Bouman et al., 2000; Bricaud and Stramski, 1990).

Although several studies have invoked photoacclimatory changes in the cell pigment content to explain part of the variability of $a^*_{ph}(\lambda)$, they have often not evaluated this effect directly (e.g., Organelli et al., 2011; Stuart et al., 1998; Wang et al., 2014). Changes in the pigment concentration per cell can be evaluated by cytometry measurements, though this approach is commonly restricted to the picophytoplankton fraction (Bricaud et al., 1999; Hickman et al., 2009; Lazzara et al., 1996; Morel et al., 1993). For the micro- and nanophytoplankton fractions, this can be assessed by combining pigment analysis and microscopic determination of cell numbers and dimensions (Brunelle et al., 2012; Fujiki and Taguchi, 2002; Stæhr et al., 2004). However, this approach is cumbersome and often difficult to operate routinely for systematic measurements in natural waters. As a result, less is known about the interactive effects of changes in the intracellular pigment concentration and cell size on pigment packaging and, therefore, on the $a^*_{ph}(\lambda)$ variability.

Here we present a comprehensive analysis of the phytoplankton light absorption variability, across the spatial and temporal scales, in offshore stratified waters of North-Western Mediterranean Sea (NWMS). The study was performed during two oceanographic cruises, right after (Sept-2011) and before (May-2012) the maxima of summer stratification. We hypothesize that, given the expected contrasting light exposure conditions (strong vertical light gradients and seasonal variations of incident solar radiation), photoacclimation (due to changes in the intracellular pigment content and/or in the proportion of accessory pigments per unit of *Chl a*) will contribute significantly to the vertical and temporal differences in $a^*_{ph}(\lambda)$. The importance of photoacclimation, in turn, will depend on the degree of variation of the phytoplankton community composition and the associated changes in the size structure. Hence, we aim at investigating the impact of photoacclimation on $a^*_{ph}(\lambda)$ variability using a suite of optical and biological parameters. To do this, we separate the effect of pigment composition from that of pigment packaging. In addition, we evaluate the use of the chlorophyll-specific beam attenuation by particles at 660 nm [$c_p^*(660)$, $m^2\ mg^{-1}$] as an optical index of phytoplankton photoacclimation (see Behrenfeld and Boss, 2003; Mignot et al., 2014; Xing et al.,

2014). With the concurrent use of c_p*(660) and the analysis of the size structure of phytoplankton community (derived from DPA approach, light microscopy phytoplankton counts and flow cytometry), we evaluate the relative contributions of the two intrinsic factors that determine the packaging effect. This study may contribute to improve our comprehension of the $a^*_{ph}(\lambda)$ variability and its main drivers with implications in a variety of bio-optical applications, such as the primary production models and the remote sensing of *chlorophyll a* concentration.

2.0 MATERIAL AND METHODS

2.1. Study area and sampling

The study was carried out in offshore waters of the NWMS (the Balearic area, over a water column depth of nearly 2000 m) during two Lagrangian cruises located in the same oceanographic system. The first on 12 - 22 September 2011 (hereinafter referred to as Sept-2011) and the second on 22 - 24 May 2012 (hereinafter referred to as May-2012) (Fig. 1).

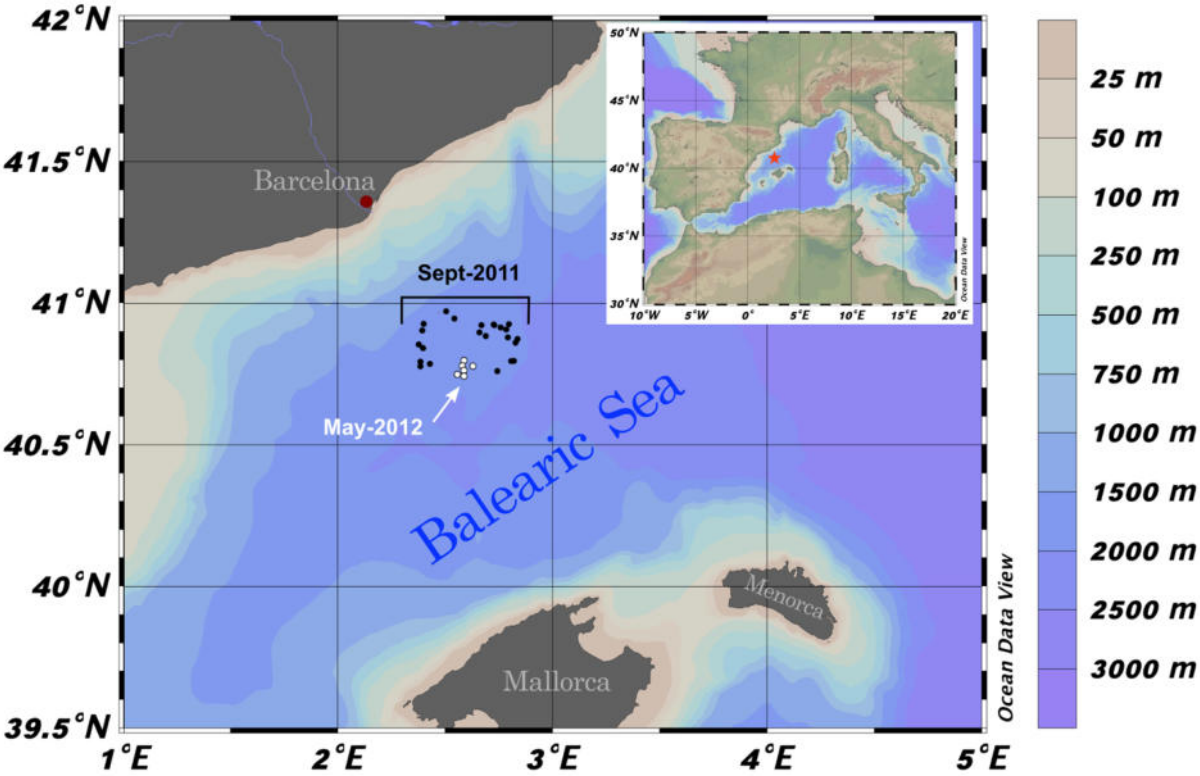

Fig. 1. Map showing the stations sampled in the two SUMMER cruises: Sept-2011 (black dots) and May-2012 (white dots).

The cruises were conducted in the framework of project SUMMER on board the RV 'García del Cid'. A CTD probe (Seabird 9/11 plus) equipped with a radiometer (QCP-2300, Biospherical), chlorophyll fluorometer (Seapoint) and C-Star transmissometer (Wet Labs, Inc.), provided depth profiles of temperature, salinity, downwelling irradiance integrated over the photosynthetically active radiation spectrum [*E*d (PAR, Z)], *Chl a* fluorescence and beam transmission. The surface mixed layer (SML) was estimated from CTD temperature profiles and its depth (Z_{SML}) was defined by a >

0.2 ºC deviation with respect to the temperature at 1 m (D'Ortenzio et al., 2005; de Boyer Montégut et al., 2004) (see Table 1 for a list of symbols, definitions and units) . The CTD system was mounted on a Niskin-bottle rosette used to collect water samples at several depths. In this study, samples of 28 stations were analysed, 22 in the longer cruise (Sept-2011) and 6 in the shorter one (May-2012). In Sept-2011 four depths were sampled (3, 8 or 10, 30 m and the deep chlorophyll maximum, DCM) and 3 depths in May-2012 (3, 25 m and DCM). The DCM was detected from fluorescence profiles and its depth (Z_{DCM}) was generally located between 45 and 60 m. Data was analysed and presented separately for three different layers. Samples at 3, 8 and 10 m corresponded to the SML, samples at 25 and 30 m to the middle layer between the mixed layer depth and DCM (hereinafter Middle), and the remaining samples to the DCM.

Symbol	Units	Description
Z_{SML}	[m]	Depth of surface mixed layer (SML)
T-Chl a	[mg m^{-3}]	Total *chlorophyll a* concentration
Fl-Chl a	[mg m^{-3}]	Calibrated profiles of fluorescence
c_p (660)	[m^{-1}]	Beam attenuation coefficient at 660 nm due to particles
c_p* (660)	[m^2 mg^{-1}]	*T-Chl a*-specific beam attenuation coefficient
*E*d (PAR)	[µmol quanta m^{-2} s^{-1}]	Downward irradiance of photosynthetically active radiation (PAR)
$\bar{E}$d (PAR)	[mol quanta m^{-2} d^{-1}]	Daily integrated underwater downward irradiance of PAR
*K*d (PAR)	[m^{-1}]	Diffuse attenuation coefficient for PAR in the euphotic layer
$Z_{1\%}$	[m]	Depth of euphotic layer (1% criterion)
Z_{DCM}	[m]	Depth of deep *chlorophyll a* maximum (DCM)
PSC	[µg L^{-1}]	Photosynthetic carotenoids concentration
PPC	[µg L^{-1}]	Photoprotective carotenoids concentration
T-APSP	[µg L^{-1}]	Total accessory photosynthetic pigments concentration
NPP index	[µg L^{-1}]	Nonphotosynthetic pigment index
a_{ph} (λ)	[m^{-1}]	Phytoplankton spectral absorption coefficient
a_{ph} (440)	[m^{-1}]	Phytoplankton absorption coefficient at 440 nm (blue band)
a_{ph} (675)	[m^{-1}]	Phytoplankton absorption coefficient at 675 nm (red band)
a^*_{ph} (λ)	[m^2 mg^{-1}]	*Chl a*-specific spectral phytoplankton absorption coefficient
a^*_{ph} (440)	[m^2 mg^{-1}]	*Chl a*-specific phytoplankton absorption coefficient at blue band
a^*_{ph} (675)	[m^2 mg^{-1}]	*Chl a*-specific phytoplankton absorption coefficient at red band
a^*_{sol} (440)	[m^2 mg^{-1}]	*Chl a*-specific total pigment absorption coefficient in solution at blue band
Q_a*(440)	[d.l.]	Pigment packaging index at 440 nm
$a^*_{ph\text{-}ppc}$ (440)	[m^2 mg^{-1}]	Photoprotective component of a^*_{ph} (440)
$a^*_{ph\text{-}psp}$ (440)	[m^2 mg^{-1}]	Photosynthetic component of a^*_{ph} (440)
F_{micro}	[d. l.]	Microphytoplankton fraction of total biomass
F_{nano}	[d. l.]	Nanophytoplankton fraction of total biomass
F_{pico}	[d. l.]	Picophytoplankton fraction of total biomass
SI	[µm]	Size index of algal population based on Diagnostic Pigment Analysis (DPA)

Table 1. Symbols used in the present study and their significance

In addition to the CTD casts, vertical profiles of downwelling spectral irradiance *E*d (λ, Z) and *E*d (PAR, Z) were determined with a PRR-800 multichannel profiling radiometer (Biospherical). Profiles were carried out around noon and recorded from the surface down to 100 m. All the irradiance profiles (with PRR-800 radiometer and CTD casts) were carried out on calm days, during clear sky and constant light conditions. Incident solar radiation in air was simultaneously monitored on deck, with an Aanderaa Instruments automated meteorological station on board. A Solar Radiation Sensor 2770 provided global radiation in the wavelength range 0.3–2500 µm. This sensor was used to derive PAR irradiance above the sea surface following Baker and Frouin (1987). The

instantaneous quantum PAR irradiance above the sea surface [Ed (PAR)$^{+0}$, μmol quanta m^{-2} s^{-1}] was calculated from W m^{-2} by multiplying by 4.60 (Kirk, 2011). The daily PAR irradiance above the sea surface [$\bar{E}$d (PAR)$^{+0}$], in mol quanta m^{-2} d^{-1}, was obtained by integrating Ed (PAR)$^{+0}$ over a day.

2.2. Apparent optical property measurements: diffuse attenuation coefficients for downwelling irradiance and related variables

Diffuse attenuation coefficients for broadband PAR [Kd (PAR)], from both CTD and PRR-800 Ed profiles, were determined as the slope of the linear regression between the logarithm of irradiance and depth, within the entire euphotic layer (from about 5 to 60 m). Prior to analysis, the data were carefully examined for irregularities (Hargreaves et al., 2007): near-surface noise caused by smooth waves and ripples was eliminated from Ed (PAR, Z) profiles. The regression analyses were statistically significant ($p<0.01$) and had R^2 above 0.98 for all evaluated casts. The depth of the euphotic layer ($Z_{1\%}$) was then calculated as 4.605/Kd (PAR), being the depth at which Ed (PAR) is reduced to 1% of its value just below the surface (Kirk, 2011). The average daily PAR irradiance for the surface mixed layer was computed in accordance with Babin et al. (1996). In addition, for the depths corresponding to the other two evaluated layers (i.e., Middle and DCM), the daily PAR irradiances were calculated from Kd (PAR) and $\bar{E}$d (PAR $^{-0}$), in accordance with Kirk (2011) as follows:

$$\bar{\mathrm{E}}d(PAR,Z) = \bar{\mathrm{E}}d(PAR^{-0}) \,.\, e^{(-kd(PAR)\,.\,Z)} \qquad (1)$$

where $\bar{E}$d (PAR $^{-0}$) is the daily downwelling PAR irradiance just beneath the air-water interface.

2.3. Inherent optical properties and related variables

Total particulate matter absorption coefficients [a_p (λ)] were determined by the quantitative filter technique (QFT), using the simple transmittance method (T-Mode) in a Lambda 800 (Perkin-Elmer) dual beam spectrophotometer (Mitchell, 1990; Mitchell and Kiefer, 1988; Trüper and Yentsch, 1967). Water samples (1 to 2 L) were filtered on-board using 25 mm-diameter GF/F filters. Immediately after filtration, absorbance scans were measured from 300 to 750 nm at 1 nm intervals. Absorbances were checked to be lower than 0.4 (Cleveland and Weidemann, 1993). The QFT method was applied according to NASA's optics protocols for absorption coefficient measurements (Mitchell et al., 2002). Spectrophotometric scans were made against a blank clean filter wetted with filtered (0.2 μm) seawater. Absorption coefficients of non-algal particles [a_{nap} (λ)] were determined with the methanol extraction method (Kishino et al.,1985). Absorption coefficients of a_p (λ) (first measurement) and a_{nap} (λ) (measurement after extraction) were estimated according to the equation:

$$a_{p,nap}(\lambda) = \frac{2.303.A_{filter}(\lambda).S}{V.\beta(\lambda)} \qquad (2)$$

where A_{filter} (λ) is the measured absorbance with QFT, S is the clearance area of the filter, V is the volume of filtered water, and β (λ) is the amplification factor vector (Mitchell and Kiefer, 1988). The β (λ) factor was calculated following Bricaud and Stramski (1990) with the equation:

$$\beta(\lambda) = 1.63\,.\,A_{filter}(\lambda)^{-0.22} \qquad (3)$$

As standard procedure, a null point correction was set at 750 nm, where absorbance by particles is assumed to be negligible. Phytoplankton absorption coefficients [$a_{ph}(\lambda)$] were obtained by subtracting $a_{nap}(\lambda)$ from $a_p(\lambda)$. The chlorophyll-specific phytoplankton absorption coefficient [$a^*_{ph}(\lambda)$] was estimated as $a_{ph}(\lambda)$/*T-Chl a*, where *T-Chl a* concentration was determined by High Performance Liquid Chromatography (HPLC) and included the following pigments (*Chl a* + allomers and epimers + *DV-Chl a* + *chlorophyllide a*) (see section 2.4.1 for details).

The packaging effect was estimated by means of the dimensionless packaging index [$Q_a^*(440)$], calculated as the ratio of the phytoplankton absorption, $a_{ph}(\lambda)$, and the absorption of total pigments in solution (without packaging) [$a_{sol}(\lambda)$] (see equation 5).

$$Q_a{}^*(440) = \frac{a_{ph}(440)}{a_{sol}(440)} \quad (4)$$

The $a_{sol}(\lambda)$ coefficient was reconstructed following the approach of Bricaud et al. (2004) (see equations 5 and 5') based on the weight-specific absorption coefficients of individual pigments proposed by Goericke and Repeta (1993) and Bidigare et al. (1990).

$$a_{sol}(\lambda) = a_{pigm}(\lambda) + a_{miss}(\lambda) \quad (5)$$

with

$$a_{pigm}(\lambda) = \sum C_i \,.\, a^*{}_i(\lambda) \quad (5')$$

where $a_{pigm}(\lambda)$ is the sum of specific absorption coefficient of the *i*-th pigment [$a^*_i(\lambda)$, $m^2\ mg^{-1}$] multiplied by their concentrations (C_i, $mg\ m^{-3}$) in the medium; and $a_{miss}(\lambda)$, the so-called missing term, depends on *T-Chl a* concentration following $a_{miss}(440) = 0.0525\ .T\text{-}Chl\ a\text{^}0.855$; (Bricaud et al., 2004). The $Q_a^*(440)$ index can vary between 0 (maximum packaging effect) to 1 (no packaging effect). The chlorophyll-specific total pigment absorption coefficient [$a^*_{sol}(\lambda)$] is defined as *T-Chl a* normalized absorption coefficient of all the pigments in solution (a_{pigm}) plus the a_{miss} term.

We also made a distinction between the part of the chlorophyll-specific phytoplankton absorption coefficient associated with photosynthetically active pigments [$a^*_{ph\text{-}psp}(\lambda)$] and that associated with nonphotosynthetic (photoprotective) pigments [$a^*_{ph\text{-}ppc}(\lambda)$] following Babin et al. (1996) (see Supplementary Material for details).

The particulate beam attenuation coefficient at 660 nm [$c_p(660)$] was calculated from 1 m binned transmittance vertical profiles and determined subtracting the mean value of beam attenuation over the depth interval from 200-400 m (representing about 70% of the signal for the layer above it). These were considered representative of the background beam attenuation of phytoplankton-free water (Loisel et al., 2011; Loisel and Morel, 1998). Particle populations in the 0.5–20 μm size range make a dominant contribution to the $c_p(660)$ signal (Boss et al., 2001; Stramski and Kiefer, 1991). This size range encompasses phytoplankton, heterotrophs, as well as detrital and inorganic particles. Nevertheless, different field studies have demonstrated that in the open ocean, to first order, the $c_p(660)$ can successfully track phytoplankton biomass (e.g., Behrenfeld and Boss, 2006; Dall'Olmo et al., 2009; Westberry et al., 2010). This was explained by either a rather constant contribution of phytoplankton to $c_p(660)$ or phytoplankton accounted for a

high proportion of c_p (660). Also, c_p (660) is less sensitive to physiological forcing (e.g., light and nutrients) than pigments, thereby engendering the ratio of c_p (660) to *T-Chl a* [c_p* (660)] with sensitivity to photoacclimation. Changes in c_p* (660) with depth and seasons have indeed been shown to follow a clear light-dependence, denoting changes in intracellular pigment concentration due to phytoplankton photoacclimation (e.g., Fennel and Boss, 2003; Mignot et al., 2014; Mitchell and Holm-Hansen, 1991). Following this, in the present study we evaluated the use of c_p (660) to track the vertical and seasonal variation in phytoplankton biomass and c_p* (660) as an optical index of phytoplankton photophysiology.

2.4. Phytoplankton pigment determinations, pigment-based phytoplankton size structure and phytoplankton identification

2.4.1. HPLC pigment determinations

Samples of 1.5 to 2 L from discrete depths were filtered through Whatman GF/F filters and stored at -80 ºC until return to the laboratory for pigment analysis. Concentrations of *T-Chl a* and accessory pigment (chlorophylls, carotenes and xanthophylls) were measured in using an HPLC instrument (Spectra SYSTEM) following the method of Zapata et al. (2000). Calibration was made using commercial pigment standards from the Institute for Water and Environment, Denmark. Vertical fluorescence profiles were first corrected, when necessary, for the Non-Photochemical Quenching effect following (Xing et al., 2012). Then, were converted into equivalent *T-Chl a* profiles (denoted *Fl-Chl a*) by using the *T-Chl a* concentration of discrete samples obtained by HPLC determinations following (Loisel et al., 2011).

In order to assess the effect of pigment composition on the variability of $a^*_{ph}(\lambda)$, we followed the pigment classification of Bricaud et al. (2004): (a) photosynthetic carotenoids [*PSC*] [fucoxanthin (*Fuco*), peridinin (*Peridi*), 19'-hexanoyloxyfucoxanthin (19'-*HF*), 19'- butanoyloxyfucoxanthin (19'-*BF*)]; (b) photoprotective carotenoids [*PPC*] [*Zeaxanthin (Zeax), Diadinoxanthin (Dd)*, *Alloxanthin (Allo)*, and *β-carotene (β-carot*)]; (c) total *Chlorophyll b* (*T-Chl b as Chl b + DV-Chl b*); and (d) total *Chlorophyll c* (*T-Chl c*). Following Babin et al. (1996), we also calculated the NPP index defined as the ratio of the concentrations of photoprotective pigments to the concentrations of total pigments

2.4.2. Pigment-based estimation of phytoplankton size classes

Diagnostic pigment analysis (DPA) (Uitz et al., 2006; Vidussi et al., 2001) was used to estimate the relative biomass proportions (*T-Chl a* fractions) of pico- (<2 µm, F_{pico}) , nano- (2–20 µm, F_{nano}) and microphytoplankton (>20 µm, F_{micro}). The biomass proportions were estimated from the concentrations of the pigments that have a taxonomic significance and can be associated with a certain size class, at least in oceanic case 1 waters. Seven pigments (i.e., *Fuco*, *Peridi*, 19'-*HF*, 19'-*BF*, *Allo*, *T-Chl b* and *Zeax*) were selected as diagnostic pigments of distinct phytoplankton groups and used to calculate the *T-Chl a* fractions belonging to the three size classes. The numerical coefficients obtained by Uitz et al. (2006), were used to compute the biomass proportions associated with each size class. It should be noted that there are some potential limitations in DPA, e.g., in some cases, a given diagnostic pigment is shared by two size classes. Despite these drawbacks, DPA is a useful approximation, and provides reasonable results at a global as well as at a regional scale. (see Supplementary Material for details).

Then, the size index (*SI*) proposed by Bricaud et al. (2004) was used to assess the variations of the dominant size class of the phytoplankton communities (see Supplementary Material for details). As already acknowledged, the *SI* index is only an approximate indicator of the dominant size of the phytoplankton assemblage (i.e., a unique central size is used to represent each size class). Besides, this metric was originally derived for samples in the first optical depth. Therefore, in this study, *SI* was only used to roughly synthesized, in a single continuous parameter, the size structure of phytoplankton community throughout the three evaluated layers.

2.4.3. Phytoplankton identification

Water samples from a random subset of CTDs (8 for Sept-2011 and 4 for May-2012) were used to describe the phytoplankton community composition. Samples of 250 mL of seawater were placed in glass bottles, preserved with formaldehyde solution (4%) and stored in the dark until analysis (within 4 months after the cruise). Micro- and nanohytoplankton were examined with an inverted microscope following the method by Utermöhl (1958). Composite chambers, after 48 hours of settling, were scanned at 125x to quantify the larger, less abundant organisms of the micro-phytoplankton, and at least two transects were examined at 312x to enumerate the smaller and more frequent nanophytoplankton forms. When possible, phytoplankton was identified to the species level, but many organisms could not be adequately classified and were pooled in categories like “Nanoflagellates 3-20 µm”, “Small dinoflagellates (<20 µm)” or “small coccolithophores (<10 µm)”.

2.4.4. Cytometric determination of picoplankton community characteristics

Determination of picophytoplankton and bacterial abundance was performed using a Becton-Dickinson FACScalibur flow cytometer (Gasol and Morán, 2015) equipped with a laser emitting at 488nm, using standard settings. Samples (1.2 mL) were fixed with a 1% paraformaldehyde and 0.05% glutaraldehyde solution and then deep-frozen in liquid N_2. Picophytoplankton samples were analysed at high speed (ca. 100 µL min^{-1}) with thresholding in red fluorescence. Three main populations *(Prochlorococcus*, *Synechococcus* and picoeukaryotes) were discriminated according to their scatter and fluorescence signals. Cell-specific pigment content was measured by the FL2 (*phycoerythrin* orange fluorescence) and FL3 (*chlorophyll a* red fluorescence) parameters (Campbell and Vaulot, 1993; Lefort and Gasol, 2014). Bacterial abundances were stained with SybrGreen I and enumerated at a low speed (ca. 15 µL min^{-1}) with thresholding in green fluorescence. The cells were identified in plots of side scatter versus green fluorescence using standard conditions (e.g., Gasol and Del Giorgio, 2000). Concentrations were obtained from weight measurement of the volume analysed. Stock solutions of 1 µm yellow-green latex beads (Polysciences) were added as an internal standard in both picophytoplankton and bacterial measurements. FL2 and FL3 content in all picophytoplankton populations were standardized to the FL2 and FL3 values of the beads to account for inter-sample machine variability.

2.5. Statistical analysis

Relationships between light exposure, pigment ratios, inherent optical properties, cell size parameters and packaging index were analysed by Spearman rank correlation analysis. This non-parametric method was chosen because environmental data often did not conform to the

requirements of parametric tests. Analyses of variance between studied environmental and bio-optical variables were performed using a one-way ANOVA test followed by the Holm–Sidak multiple pairwise comparison method to determine significance of differences between both cruises and layers. In the case of non-normal distributions, the non-parametric Kruskal-Wallis test was utilized. Graphs and statistics were performed with R software (R Development Core Team, 2004). Figure 1 and 2 were plotted using Ocean Data View (ODV) software (version 5.0, Schlitzer, R., Ocean Data View, https://odv.awi.de, 2018).

3.0 RESULTS

3.1. Characteristics of the study area: continuous vertical profiles of temperature, irradiance, *chlorophyll a,* and beam attenuation

Both cruises presented shallow SML with mean depths of 11.8 ± 4.0 m and 18.2 ± 1.5 m in Sept-2011 and May-2012, respectively. Sea surface temperature was on average 7 °C higher during Sept-2011. The thermally homogeneous layer was well above the limit of the euphotic depth (situated around 60 m), delimiting from the bottom of the SML up to $Z_{1\%}$ a sunlit, stratified layer (Fig. 2a, c and Fig. 3a, b). In the SML, similar *T-Chl a* concentration was observed between cruises, with only slightly higher mean values in May-2012 (Table S1).

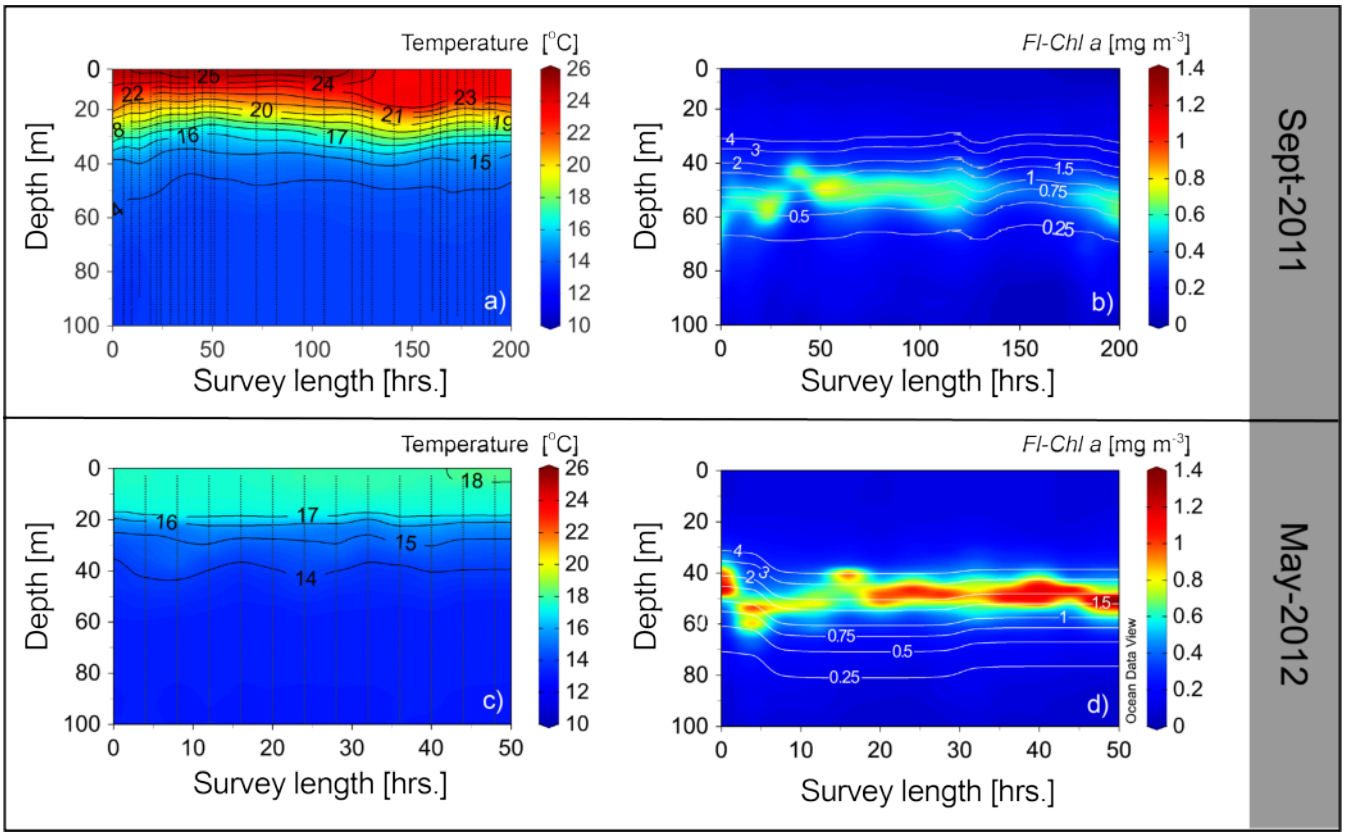

Fig. 2. Cross sections of temperature with isotherms every 1 °C (a, c) and HPLC converted *chlorophyll a* fluorescence (*Fl-Chl a*) (b, d). In subplots a) and c) small black dots represent the 1m binned CTD data at each sampling station. In subplots b) and d) the white solid lines are the isolumes (in mol quanta m^{-2} d^{-1}) near the DCM level. Note the different interval length in x- axis scales between Sept-2011 (subplots a and b) and May-2012 cruises (subplots c and d).

The DCMs were well developed during both cruises, situated in the stratified part of the water column. Nevertheless, clear inter-cruise differences in either DCM magnitude or vertical distribution were observed. In Sept-2011, the DCM displayed on average 1.6-fold lower *T-Chl a* concentration (Table S1) and a significantly deeper vertical position (Z_{DCM} = 54.1 ± 4.5 m in Sept-2011 and 47.5 ± 2.2 m in May-2012, ANOVA, $p<0.05$) (Fig. 2c, d and Fig. 3a, b).

Inter-cruise differences in incident solar radiation, explained by the solar seasonal cycle, resulted in dissimilar light exposure along the stratified water column. The Sept-2011 cruise presented a 22% lower mean values of incident daily PAR irradiance at the sea surface. Significant differences in $\bar{E}d$ (PAR) occurred between cruises at the Middle and DCM depths (ANOVA, $p\leq0.003$). In Sept-2011 the DCM was placed at isolumes (the level where the daily integrated photon flux is constant) between 0.5 and 2 mol quanta m^{-2} d^{-1} (mean value of 0.72 ± 0.28), while in May-2012 the DCM was placed at higher isolumes between 0.75 and 4 mol quanta m^{-2} d^{-1} (mean value of 1.43 ± 0.6) (Fig. 2c, d; Fig. 3b; Table S1).

In addition to the observed vertical structure of *T-Chl a*, both cruises showed an uneven distribution of c_p (660) with a pronounced deep maximum about 5 meters above the DCM (Fig. 3c). The average values of c_p (660) increased from the SML to the DCM by a factor between 2.3 and 3 in the two surveys. In contrast, *T-Chl a* depicted a much steeper increase, resulting in a significantly decrease with depth by a factor of ~4 of c_p* (660) (ANOVA, $p<0.001$) (Table S1; Fig. 3d). The relationship between c_p (660) and *T-Chl a* is further illustrated in Fig. S1. Superimposed to the regular vertical structure of either c_p (660) or c_p* (660), clear differences between cruises were also found. The mean values of c_p (660) and c_p* (660) were significantly higher in May-2012 in the three examined layers (ANOVA, $p\leq0.005$) (Table S1; Fig. 3c, d).

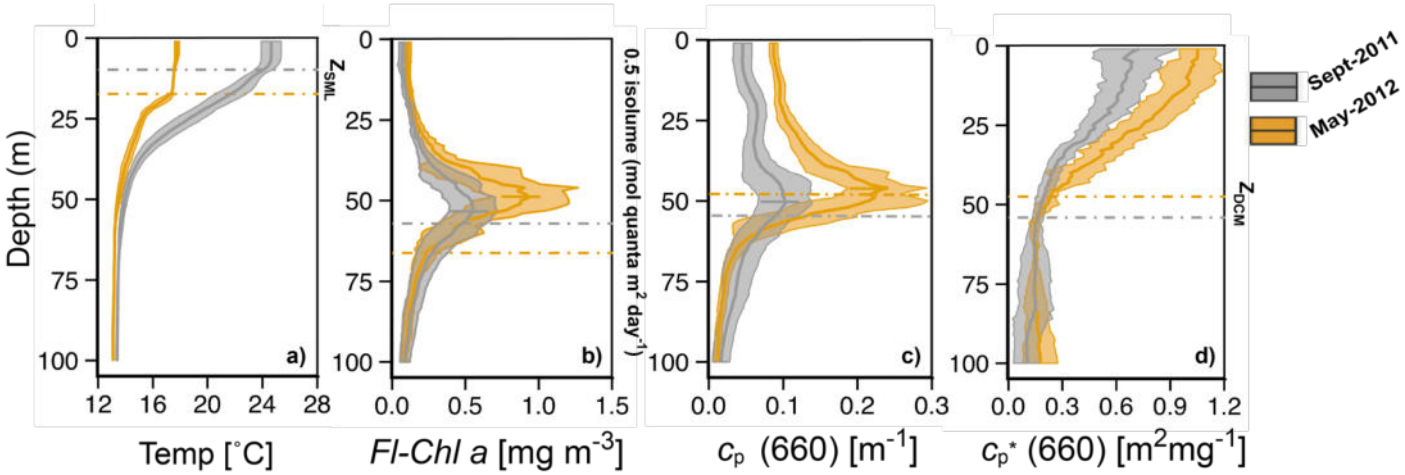

Fig. 3. The average depth distribution of (a) temperature, (b) corrected *chlorophyll a* fluorescence [*Fl-Chl a]*, (c) beam attenuation by particles [c_p (660)] and (d) chlorophyll-specific beam attenuation [c_p* (660)] for the Sept-2011 (22 stations) and May-2012 (6 stations) cruises. Shaded areas represent ±1 SD. In subplot (a), the depth of SMLs is indicated with horizontal dashed lines. In subplot (b) the dashed lines indicate the 0.5 isolumes. In subplots (c and d) the dashed lines indicate the depth of DCMs.

3.2. Variation in the phytoplankton pigment composition and community structure

The contributions of the four groups of accessory pigments (i.e., *PSC*, *PPC*, *T-Chl b* and *T-*

356 *Chl c*), relative to *T-Chl a* concentration, were variable in the different layers and between cruises
357 (Fig. 4, see section 2.4. and Table 1 for symbols and definitions). The *PSC:T-Chl a* ratio showed an
358 even vertical distribution in Sept-2011, but a clear and significant increase (up to 17%) with depth in
359 May-2012 (ANOVA, p = 0.008) (Fig. 4a; Table S1). In Sept-2011, *PSC:T-Chl a* was mostly
360 determined by the *19'-HF:T-Ch a* ratio (Table S1). In May-2012, both the *19'-HF:T-Ch a* and *19'-*
361 *BF:T-Ch a* ratios increased with depth and mainly explained the *PSC:T-Chl a* vertical trend.

362 In contrast, the *PPC:T-Chl a* ratio showed a steeper and significant decrease with depth in
363 both cruises (ANOVA, p≤0.005), (Fig. 4b; Table S1). This decrease was mostly determined by the
364 *Zeax:T-Chl a* ratio in Sept-2011 and by the *Dd:T-Chl a* ratio in May-2012 (Table S1). Similarly, values
365 of NPP (the ratio of non-photosynthetic pigments to total pigment concentration) were significantly
366 higher than those at the DCM (ANOVA, p≤0.005) (Table S1). The *PPC:T-Chl a* ratio was significantly
367 higher in Sept-2011 than in May-2012 at the three evaluated layers (ANOVA, p≤0.02); despite higher
368 irradiances in the latter cruise. In contrast, the *PSC:T-Chl a* ratio was only significantly higher in
369 May-2012 at the DCM layer (ANOVA, p = 0.0011) (Table S1).

370 The accessory chlorophylls (*T-Chl b* and *T-Chl c*) to *T-Chl a* ratios increased significantly with
371 depth in both cruises (ANOVA, p≤0.005), (Fig. 4c, d; Table S1), and so did the ratios of the total
372 accessory photosynthetic pigments (i.e., *PSC* + *T-Chl b* + *T-Chl c*, herein after *T-APSP*) (ANOVA,
373 p≤0.005) (Table S1). Between cruises, *T-Chl b:T-Chl a* was higher in Sept-2011, and *T-Chl c:T-Chl*
374 *a* was higher in May-2012, for the three evaluated layers. No differences were found in the *T-*
375 *APSP*:*T-Chl a ratio.*

376 The diagnostic pigment data also revealed important vertical and inter-cruises differences in
377 the phytoplankton community structure. The *19'-HF* was the most abundant carotenoid in the entire
378 water column of both cruises, accounting on average for 30% and 38% of total carotenoids in Sept-
379 2011 and May-2012, respectively. This suggests that prymnesiophytes were the dominant group of
380 phytoplankton. On the other hand, *Fuco* was found in low amounts during both cruises (<10% of
381 total carotenoids). The surface waters of Sept-2011 also presented high concentrations of *Zeax,*
382 which accounted for 29% of the total carotenoids. This is indicative of a high abundance of
383 *Synechococcus spp*., because diagnostic pigments of green algae (*Viola, Lut* and *Prasino)*, that also
384 contain *Zeax*, were found in low abundance at the SML of this cruise. Besides, the contribution by
385 *Prochlorococcus spp*., another *Zeax* producer, was deemed unimportant because *DV-Chl a* was
386 only 7% of *T-Chl a* in the SML. In contrast, the SML of May-2012 presented important concentrations
387 of *19'-BF and Dd.* The latter two pigments accounted for 35% of the total carotenoids, indicating
388 also the presence of chrysophytes/pelagophytes. *Zeax* was comparatively less abundant in this
389 cruise (<9% of total carotenoids), suggesting lower relative abundance of Cyanobacteria. Other

pigments like *DV-Chl a* and *Prasino* were undetected in the SML of May-2012.

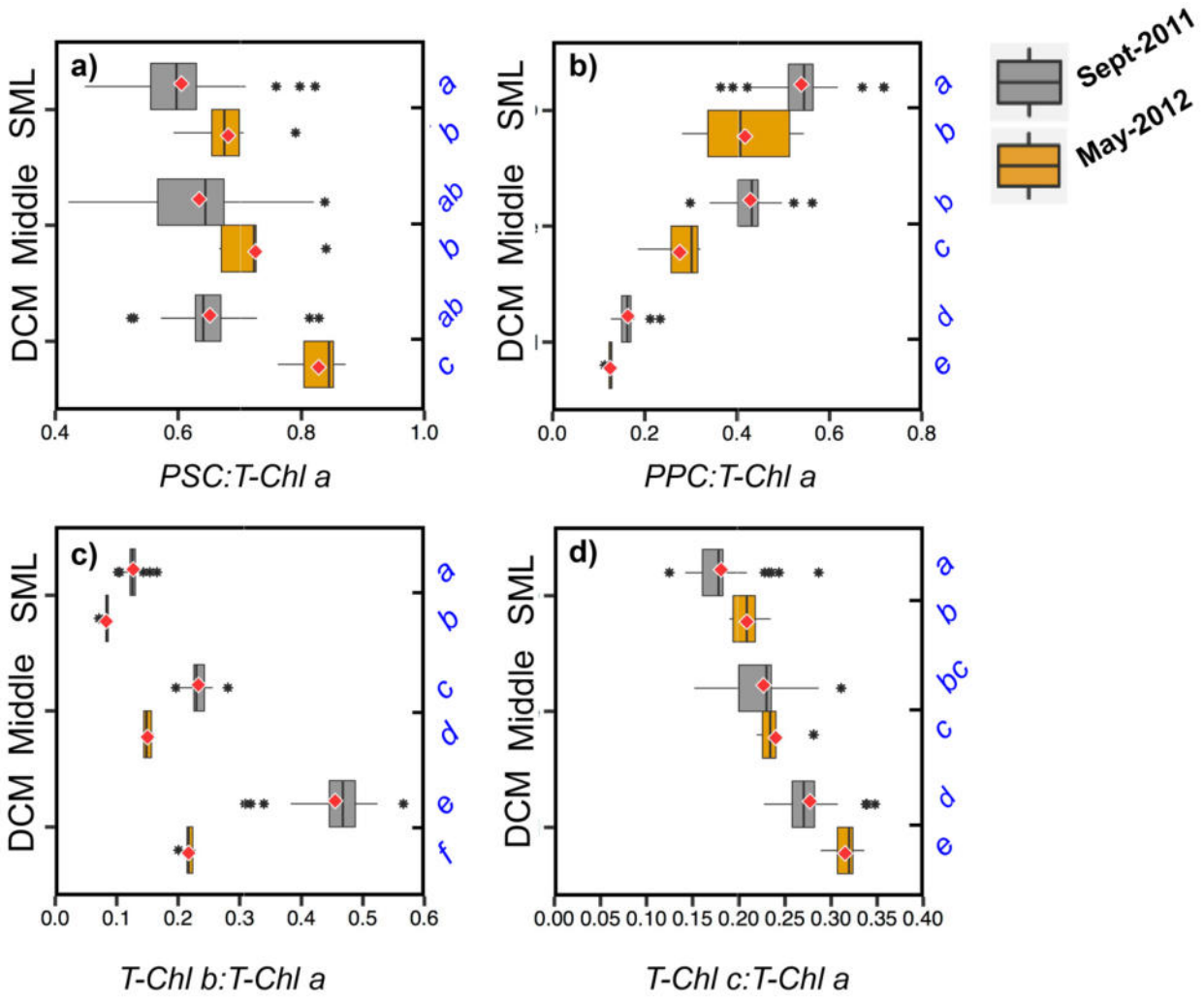

Fig. 4. Distribution of the ratios *PSC:T-Chl a* ratio) (a); the *PPC:T-Chl a* ratio (b); the *T-Chl b:T-Chl a* ratio (c) and the *T-Chl c:T-Chl a* ratio for the three evaluated layers during the SUMMER cruises. The distributions are presented as boxplots where the central line is the median of the distribution of data and the red diamond is the mean; the edges of the boxes denote the 25th and 75th percentiles, while the whiskers denote the 10th and 90th percentiles; black asterisks represent outliers. Levels connected with the same blue letter were not significantly different at a p>0.05 after ANOVA test.

In the vertical dimension, the Sept-2011 cruise was characterized by an increase *of DV-Chl a* at the Middle and DCM layers, accounting for up to 24% of *T-Chl a* at the DCM level and indicating high abundances of *Prochlorococcus spp*. *T-Chl b* showed an even steeper increase with depth (Table S1). The vertical trends of *DV-Chl a* and *T-Chl b* would indicate both a change in phytoplankton composition and the acclimation of *Prochlorococcus spp.* cells to low irradiance. DCMs of Sept-2011 also showed significant concentrations of *19'-BF* (accounting for 22% of total carotenoids), increasing their proportion relative to *19'-HF*. This is indicative of an increase in the relative importance of chrysophytes/pelagophytes vs. prymnesiophytes towards the base of the euphotic layer.

May-2012 showed less vertical variation in the proportion of taxonomic pigment

concentrations than Sept-2011. The DCM layer was characterized by high abundances of prymnesiophytes (*19'-HF* accounting for the 44% of total carotenoids) and high concentrations of *19'-BF* and *T-Chl c*. The carotenoid *19'-BF*, as in the Sept-2011, increased its proportion relative to *19'-HF* with depth. In addition, the observed increase in the *T-Chl b:T-Chl a* ratio at the DCM would suggest higher abundances of green algae (including prasinophytes), because *DV-Chl a*, a marker pigment of prochlorophytes, was only present at low concentrations (Table S1).

Light microscopy observations confirmed the scarcity of large diatoms (less than 2% of cell abundance) and the dominance of nanoflagellates (60-70%) in both cruises. Besides, naked small dinoflagellates (<20 μm) contributed on average to 35 and 28% of total cell counts in Sept-2011 and May-2012, respectively. Significant vertical and inter-cruise differences in the phytoplankton cell counts were observed (ANOVA, $p<0.001$). SML presented around 3.5-fold lower mean cell abundance than the DCM in both cruises. Besides, May-2012 presented around 5-fold higher mean cell abundance (9.2 10^4 cell L^{-1}) than Sept-2011 (1.9 10^4 cell L^{-1}). In addition, enumerations by flow cytometry supported in general pigment analysis of picophytoplankton (Table 2). Photosynthetic prokaryotes (*Prochlorococcus* + *Synechococus*) were more abundant at the three evaluated layers in Sept-2011. Besides, a clear increase of *Prochlorococcus* abundance was observed bellow SML in both cruises, with higher values in Sept-2011. The cytometry standardized fluorescence parameters: *phycoerythrin* orange fluorescence (FL2) and *chlorophyll a* red fluorescence (FL3), which indicate the cell-specific pigment content, increased towards the DCM (Table 2). In May-2012, *Synechococus* (which constituted more than 80% of the picoplankton abundance in this cruise) showed lower relative fluorescence than in Sept-2011. Variation between cruises was less clear for *Prochlorococcus spp.* and picoeukaryotes, which only during May-2012 showed slightly lower FL3 values at the DCM level (Table 2). Regarding heterotrophic bacteria, no significant differences in the bacteria:*T-Chl a* ratio were observed between cruises (ANOVA, $p<0.005$).

Cruise	*Sept-2011*			*May-2012*		
	Average (± SD)			Average (± SD)		
Layers	**SML**	**Middle**	**DCM**	**SML**	**Middle**	**DCM**
Synechococcus						
Abundance (10^4 cells ml^{-1})	2.94 (± 0.59)	2.31 (± 0.26)	1.02 (± 0.86)	3.03 (± 3.53)	3.53 (± 4.85)	2.88 (± 1.41)
FL2 (rel. units)	0.07 (± 0.02)	0.19 (± 0.05)	2.58 (± 0.68)	0.06 (± 0.03)	0.05 (± 0.01)	1.57 (± 1.08)
FL3 (rel. units)	0.59 (± 0.13)	1.29 (± 0.31)	13.01 (± 3.42)	0.28 (± 0.04)	0.27 (± 0.02)	5.41 (± 2.18)
Prochlorococcus						
Abundance (10^4 cells ml^{-1})	1.80 (± 1.20)	9.45 (± 2.81)	5.98 (± 2.90)	0.23 (± 0.54)	0.22 (± 0.26)	0.98 (± 0.20)
FL3 (rel. units)	0.05 (± 0.01)	0.09 (± 0.02)	1.12 (± 0.36)	0.29 (± 0.10)	0.24 (± 0.07)	1.07 (± 0.47)
Picoeukariotes						
Abundance (10^4 cells ml^{-1})	0.12 (± 0.04)	0.11 (± 0.03)	0.15 (± 0.11)	0.16 (± 0.03)	0.17 (± 0.03)	0.22 (± 0.05)
FL3 (rel. units)	8.13 (± 1.15)	10.90 (± 2.20)	26.27 (± 5.79)	12.95 (± 3.06)	16.94 (± 5.01)	24.60 (± 7.97)
Bacteria Abundance (10^5 cells ml^{-1})	4.90 (± 1.70)	5.09 (± 1.58)	4.73 (± 1.91)	5.02 (± 1.63)	5.65 (± 2.06)	8.36 (± 2.73)

Table 2. Average values of different picoplankton community parameters and that of heterotrophic bacteria abundance. FL2 and FL3 stand for *phycoerythrin* orange fluorescence and *chlorophyll a* red fluorescence, respectively.

3.3. Variation of phytoplankton absorption coefficients

Over the entire water column, a_{ph} (440) varied from 0.005 to 0.063 m^{-1} and from 0.008 to 0.103 m^{-1} in Sept-2011 and May-2012, respectively. The values of a_{ph} (675) ranged from 0.001 to 0.023 m^{-1} in Sept-2011 and from 0.002 to 0.042 m^{-1} in May-2012. As reported in previous studies, a_{ph} (440) and a_{ph} (675) were positively and significantly ($p<0.001$) related to *T-Chl a* following a power-law functions. For a_{ph} (440), the function was: a_{ph} (440) = 0.062 *T-Chl a* $^{0.785}$ (R^2 = 0.95, $p<0.0001$, n= 98) (Fig. 5). This relationship is akin to the global average relationships reported by Bricaud et al. (1998, 1995), but shows a steeper slope. The slope of our relationship is closer to that obtained by Organelli et al. (2011) in the Mediterranean Sea over a similar *T-Chl a* range, but our a_{ph} (440) measurements are ~15% higher (Fig. 5).

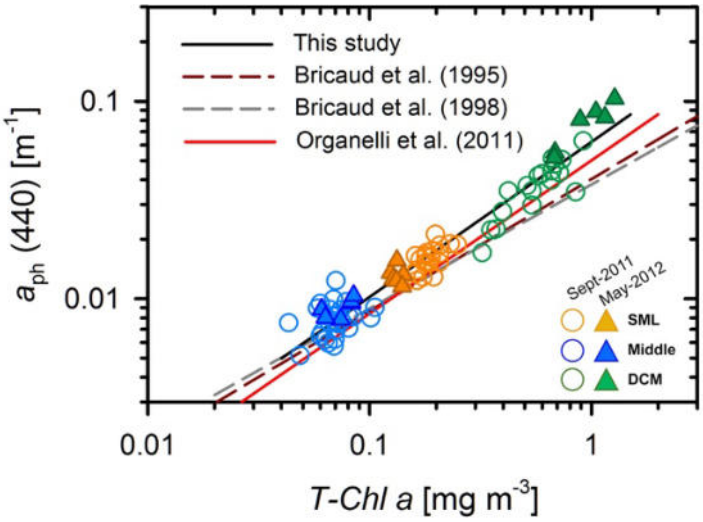

Fig. 5. The phytoplankton absorption coefficient at 440 nm as a function of *T-Chl a* concentration. The black solid line represents the best fit regression (power law function) between a_{ph} (440) and *T-Chl a* (see text) considering both cruises and the three evaluated layers of this study. The relationships from Bricaud et al. (1995) (burgundy dashed line), Bricaud et al. (1998) (grey dashed line) and Organelli et al. (2011) (red solid line) are also displayed for comparison.

In addition, important vertical and inter-cruise variations in the chlorophyll-specific absorption coefficients were observed. Considering the entire data set, the ranges of a^*_{ph} (440) and a^*_{ph} (675) were 0.041-0.174 m^2 mg^{-1} and 0.014-0.051 m^2 mg^{-1}, respectively. Both cruises showed a clear vertical decrease of a^*_{ph} (440) (Fig. 6c, d; Table S1), with average values significantly different between the SML and the DCM (ANOVA, $p \leq 0.005$) (Fig. 7a). In Sept-2011, the mean surface value of a^*_{ph} (440) was ~1.7-fold higher than at the DCM, while in May-2012 this difference was about ~1.5-fold (Table S1). Vertical variation was less marked for a^*_{ph} (675) (Table S1). In addition, values of a^*_{ph} (440) and a^*_{ph} (675) were always lower in Sept-2011 than in May-2012 (Table S1).

The vertical gradients of both a_{ph} (λ) and a^*_{ph} (λ) were accompanied by changes in the shape of the absorption spectra (Fig. 6). The a_{ph} (λ) spectra, when normalized with respect to a_{ph} (440), progressively increased around 470-480 nm and ~650 nm from the SML to the DCM (Fig. 6e, f). This can be attributed to the observed increase of accessory chlorophylls with depth. A strong correlation was found between a_{ph}(475):a_{ph}(440) and *T-Chl b*:*T-Chl a* in Sept-2011 (R=0.81,

454 p<0.001, n=81) and between $a_{ph}(475)$:$a_{ph}(440)$ and (*T-Chl b +T-Chl c):T-Chl a* in May-2012 (R=0.90,
455 p<0.001, n=17). In addition, an absorption increase between 515-533 nm was also evident towards
456 deeper waters in May-2012 (Fig. 6f), likely related to the vertical trend of the *19'-BF:T-Chl a + 19'-*
457 *HF:T-Chl a* ratio (R=0.74, p<0.001, n=17).
458

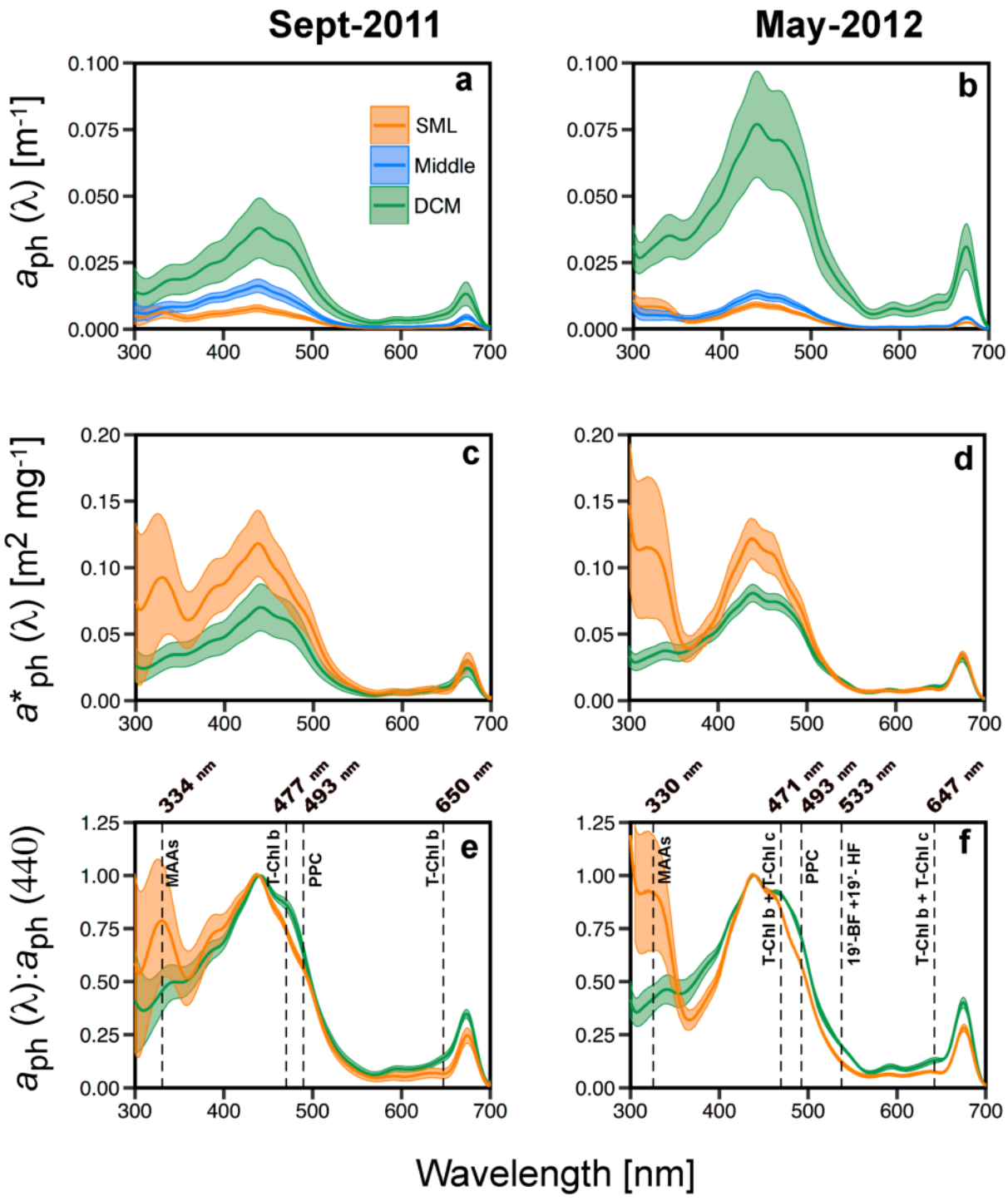

Fig. 6. Mean values of phytoplankton absorption spectra [a_{ph} (λ)] (a, b); chlorophyll-specific phytoplankton absorption [a^*_{ph} (λ)] (c, d) and phytoplankton absorption spectra normalized at 440 nm [a_{ph} (λ): a_{ph} (440)] (e, f), for the three evaluated layers in the Sept-2011 and May-2012 cruises (in c, d, e and f, the Middle layer was omitted for clarity). Shaded areas represent ± 1 standard deviation.

Although masked by the overlapping with chlorophyll absorption bands, an absorption shoulder around 490 nm associated to PPC was identified in SML samples (Fig. 6e, f). This shoulder progressively vanished with depth, reflecting the vertical decrease of *PPC:T-Chl a* in both cruises. In Sept-2011 the $a_{ph}(493):a_{ph}(440)$ ratio was positively correlated with *Zeax:T-Chl a* (R=0.63, p<0.001, n=81). Differences in a_{ph} (λ) spectral shape were also evidenced by analysing the Blue:Red ratio [i.e., a_{ph} (440):a_{ph} (675), hereinafter B:R]. The B:R ratio was significantly higher at the surface (~30%) than at the DCM in both cruises (ANOVA, p<0.001). These differences can be explained by the varying proportions of *PPC*, being the B:R ratio positively and strongly related with the *NPP* index (R=0.79, p<0.0001, n=98). Besides, special features were also detected in the UV spectral region, indicating the presence of the UV sunscreens Mycosporine-like amino acids.

3.4. Partitioning phytoplankton absorption: contribution of photoprotective and photosynthetic fractions to a^*_{ph} (440) variation

The partitioning analysis, which takes into account the effects of pigment composition and packaging, showed that the absorption associated to the photoprotective pigments, $a^*_{ph\text{-}ppc}$ (440), represented about 30% of a^*_{ph} (440) in the SML of both cruises, but was a minor component at the DCM (~10%) (Table S1). Alike for a^*_{ph} (440), the $a^*_{ph\text{-}ppc}$ (440) and $a^*_{ph\text{-}psp}$ (440) (the absorption by photosynthetic fraction) also showed a significant decrease with depth in both cruises (ANOVA, p≤0.005) (Fig. S2 and Fig. 7a, b and c). Surface $a^*_{ph\text{-}ppc}$ (440) was 3.8 and 4.7-fold higher than at the DCMs in Sept-2011and May-2012, respectively (Table S1). On the other hand, $a^*_{ph\text{-}psp}$ (440) presented a less pronounced vertical pattern, with mean values 1.3 and 1.2-fold higher at the surface in Sept-2011 and May-2012, respectively (Table S1; Fig. 7b and c).

Therefore, around 60% of the observed a^*_{ph} (440) decrease with increasing depth was accounted for by changes in the photoprotective fraction of phytoplankton absorption. This was also supported by the significant positive relationship between a^*_{ph} (440) and the *PPC:T-Chl a* ratio (R= 0.72, p<0.0001, n=81 and R=0.83, p<0.0001, n=17 in Sept-2011 and May-2012, respectively). In contrast, the total accessory photosynthetic pigments to *T-Chl a* ratio, *T-APSP:T-Chl a*, increased towards the DCM (Table S1). Therefore, the modest vertical decrease observed for the photosynthetic fraction (Fig. 7c and Fig. S2c) indicates that the packaging effect is also an important driver of a^*_{ph} (440) vertical variation. This is further analysed in section 3.5.

Inter-cruise differences in a^*_{ph} (440) were mainly attributed to the photosynthetic fraction of phytoplankton absorption. While differences between cruises for the photoprotective absorption fraction was minor (with slightly higher values during Sept-2011, Fig. 7b), we observed significantly lower mean values of the photosynthetic fraction in Sept-2011 than in May-2012 at the three depths (ANOVA, p<0.008) (Fig. 7c). The *T-APSP:T-Chl a* ratio, however, did not show significant differences between surveys throughout the illuminated water column (Table S1), indicating that a lower packaging effect in May-2012 (Fig. 7e) was responsible for the observed inter-cruise variation of a^*_{ph} (440).

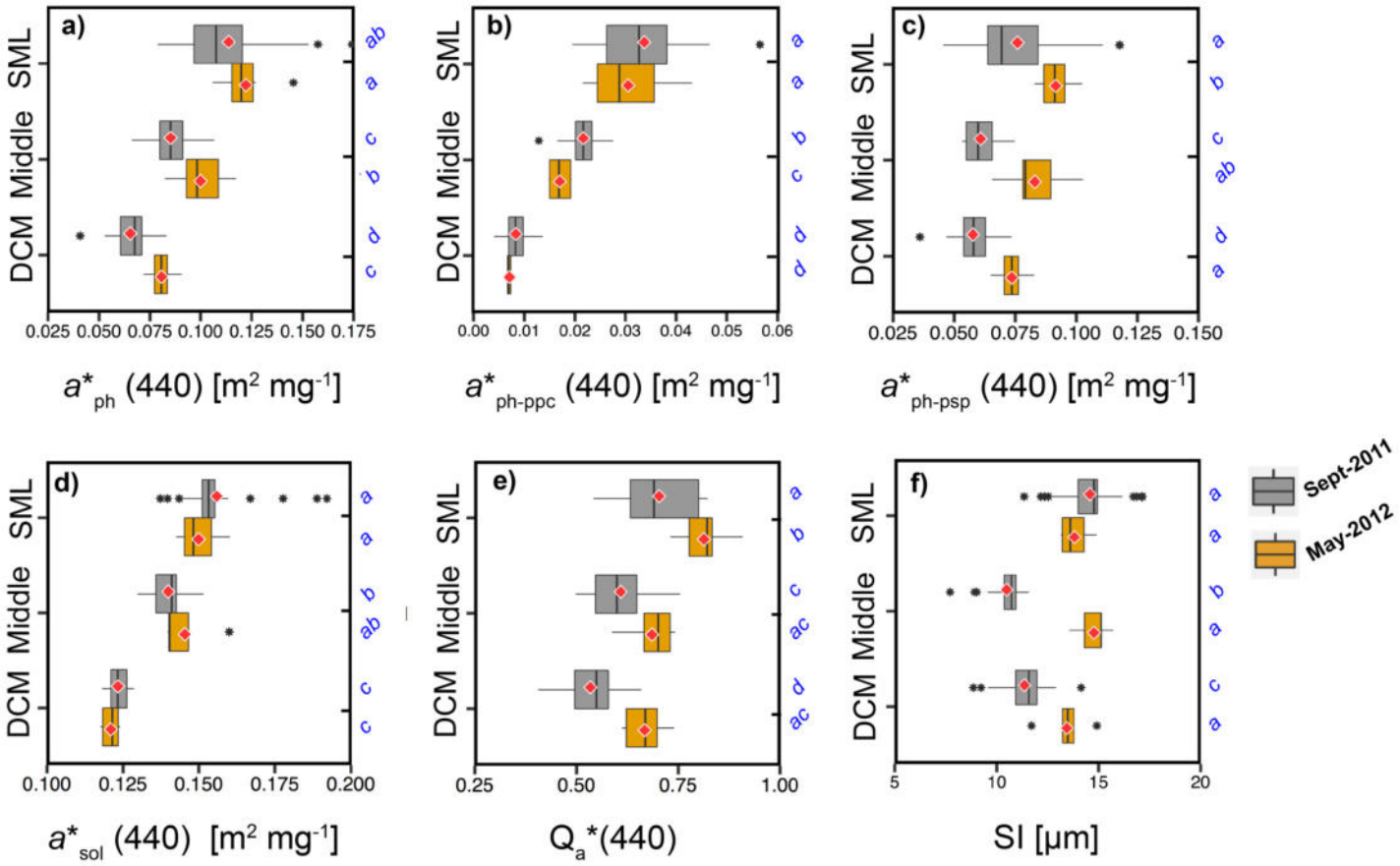

Fig. 7. Distribution of the phytoplankton chlorophyll-specific absorption coefficient, a^*_{ph} (440) (a); the photoprotective absorption fraction, $a^*_{ph\text{-}ppc}$ (440) (b); the photosynthetic absorption fraction, $a^*_{ph\text{-}psp}$ (440) (c); the chlorophyll-specific absorption of total pigments in solution (without packaging), a^*_{sol} (440) (d), the packaging index, Q_a^*(440) (e) and the size index, *SI* (f) for the three evaluated layers in the SUMMER cruises. Description of the boxplots as in Figure 4

3.5. Effects of pigment composition and packaging on a^*_{ph} (440) variability

Values of a^*_{sol} (440), which indicate the unpackaged absorption of pigments, presented a moderate decrease with depth in both cruises (Fig. 7d; Table S1). This pattern resulted from the partial compensation between photosynthetic and photoprotective pigments that displayed opposite vertical patterns (see Fig. 4). The strong signature of photoprotective pigments through the illuminated water column remains evident, with mean surface values of a^*_{sol} (440) significantly higher (~1.25-fold) than at the DCMs in both cruises (ANOVA, $p<0.005$) (Fig. 7d; Table S1).

By comparing the vertical profiles of a^*_{ph} (440), a^*_{sol} (440) and packaging index [remember that Q_a^* (440) = a_{ph} (440) / a_{sol} (440)], we estimated that about half of the variation in the mean values of a^*_{ph} (440) between the SML and the DCM were explained by differences in pigment composition. The depth decreases of a^*_{sol} (440), ruled by photoprotective pigments, explained about 46% and 52% of a^*_{ph} (440) vertical variation in Sept-2011 and May-2012, respectively. The remaining variation was consequently attributed to the packaging effect. In both cruises, the Q_a^* (440) index showed a significant decrease with depth (ANOVA, $p \leq 0.008$), with surface values 1.3

511 and 1.2-fold higher (i.e., lower packaging) than at the DCMs of Sept-2011 and May-2012,
512 respectively (Table S1; Fig. 7e).

513 The minor inter-cruise differences in the average $a^*_{sol}(440)$ at the three depths (Fig. 7d; Table
514 S1) indicate that temporal differences in $a^*_{ph}(440)$ were caused by the different degrees of pigment
515 packaging. A similar conclusion can be deduced from the comparative analysis of $a^*_{ph\text{-}ppc}(440)$ and
516 $a^*_{ph\text{-}psp}(440)$ (section 3.4). Indeed, the mean values of $Q_a^*(440)$ were ~15% lower in Sept-2011 than
517 in May-2012 at both the SML and DCM (ANOVA, $p<0.05$) (Fig. 7e), indicating a stronger packaging
518 effect and explaining the lower values of $a^*_{ph}(440)$ in Sept-2011.

519

520 **3.6. Understanding the packaging effect: the effects of the size structure and intracellular**
521 **pigment concentration of the phytoplankton community**

522 The DPA used to derive the size structure of the phytoplankton community was in general in
523 good agreement with the light microscopy phytoplankton counts and cytometry determinations.
524 During Sept-2011 waters were co-dominated by picophytoplankton (42%) and nanophytoplankton
525 (38%), with a lower contribution of microphytoplankton (20%). In contrast, during May-2012 waters
526 were generally dominated by nanophytoplankton (57%), with lower contributions of pico and
527 microphytoplankton (~22% each) (Table S1). In both cruises, the fraction of picophytoplankton
528 biomass increased by around 20% from the SML to the DCM. Values of *SI* index varied in a narrow
529 range with mean values between 10 and 15 μm. In Sept-2011, surface waters had a higher mean
530 *SI* than the DCM (ANOVA, $p<0.001$), while no significant vertical differences occurred in May-2012.
531 Differences in *SI* were also observed between cruises, with lower mean *SI* values in Sept-2011 than
532 May-2012 at the Middle and DCM depths (ANOVA, $p<0.001$) (Fig. 7f; Table S1).

533 By comparing the figure 7e and the derived joint information of DPA, *SI* index, light microscopy
534 observations and flow cytometry, we can see that neither the vertical patterns of $Q_a^*(440)$ nor its
535 differences between cruises can be explained by differences in the size structure of phytoplankton
536 community. Namely, during Sept-2011 the phytoplankton of the DCM, even though presenting
537 higher proportions of picophytoplankton and lower of microphytoplankton (i.e., small cells), had their
538 pigments more packaged [lower $Q_a^*(440)$] than phytoplankton at the SML (Table S1 and Fig 7e).
539 Likewise, the phytoplankton assemblages of Sept-2011 had more packaged pigments than in May-
540 2012, despite the community size structure in the latter cruise was composed by a lower proportion
541 of picophytoplankton (i.e., higher cells) (Table S1; Fig. 7e).

542 The other factor responsible for the packaging effect is the per cell concentration of pigments.
543 Using $c_p^*(660)$ as an optical index to track changes in phytoplankton photophysiology, we were able
544 to explain much of the variability of $Q_a^*(440)$ ($R=0.755$, $p<0.001$, $n=98$) (Fig. 8). Photoacclimation,
545 either to the decreasing light availability through the water column or to the inter-cruise seasonal
546 variation of solar irradiance, resulted in a higher intracellular *T-Chl a* concentration and stronger

pigment packaging [lower values of c_p* (660) and Q_a*(440)] with depth in both cruises, and during Sept-2011 relative to May-2012.

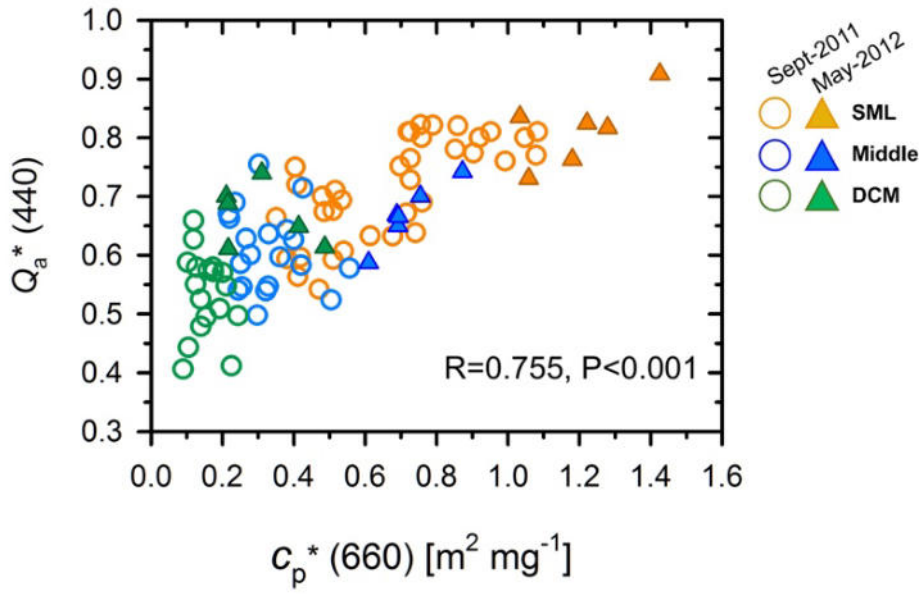

Fig 8. The relationship between the packaging effect index [Q_a* (440)] and the chlorophyll-specific beam attenuation by particles [c_p* (660)].

4.0. DISCUSSION

4.1 Vertical and inter-cruise differences in c_p (660), *T-Chl a* and their relationship

The SUMMER cruises took place at the end (Sept-2011) and the beginning (May-2012) of the stratified season in the NWMS. Although both cruises had similarly low *T-Chl a* concentration in the SML, the late-spring cruise (May-2012) presented on average 2-fold higher c_p (660) in the euphotic layer. This difference is likely indicative of higher phytoplankton biomass (in terms of carbon) in the latter cruise and could be explained by the hydrographic structure and the seasonality of nutrient concentrations. In the NWMS, the nitracline depth is maximal during July-September, when the water column is nitrate-depleted down to about 60 m. Conversely, shortly after the onset of stable stratification (March-May) the nitracline is shallower (<40 m) and turbulent mixing events can entrain nutrients into the upper layer (Pasqueron de Fommervault et al., 2015), enhancing phytoplankton biomass production.

In SUMMER cruises, the distinctive patterns of c_p (660) and *T-Chl a* resulted in clear vertical and inter-cruise differences in c_p* (660) (a proxy for Carbon: *Chl a* ratio). Remarkably, these differences in c_p* (660) were coincident with either the depth decreasing light availability or the lower mean daily PAR irradiance in the euphotic layer of Sept-2011, most likely indicating differences in phytoplankton photoacclimation. Related to the latter, a noteworthy feature of our observations was the position of DCM in terms of available light in absolute values. The benchmark study of Letelier et al. (2004) showed that, in some cases, the DCM seasonal dynamics were essentially irradiance driven. Our observations, conversely, indicate that DCM displacement also coincide with a change of isolume, indicating that other factors were also involved (see Cullen, 2015). These outcomes are

in agreement with contemporary works that observed seasonal differences in the photon flux at the DCM (Barbieux et al., 2019; Lavigne et al., 2015; Mignot et al., 2014). Besides, the temporal differences in the position and amplitude of the DCM described here are coincident with previous observations in the NWMS (e.g., Estrada et al., 2014).

Even if different field studies have demonstrated that, to first order, the c_p (660) can track phytoplankton biomass (see Dall'Olmo et al., 2009, and references therein), the drawback of using c_p (660) is that it is not unique to phytoplankton. In the present study, however, we have evidence supporting the idea of vertical and inter-cruise differences in phytoplankton biomass and photoacclimation. First, we did not register important differences in the heterotrophic bacterial abundance between cruises, with only higher values at the DCM of May-2012, but no significant differences in bacteria:*T-Chl a* were observed. Second, light microscopy observations showed important inter-cruise differences in the total phytoplanktonic cell counts with around 5-fold higher mean cell abundance in May-2012 than in Sept-2011. Besides, these differences in cell counts were higher than inter-cruise differences in *T-Chl a* concentration, indicating lower intracellular pigment concentration during May-2012 than Sept-2011. Furthermore, in the vertical dimension and in both cruises, a higher depth increases of *T-Chla* concentration than that of the total cell abundance explained the higher pigment concentration per cell towards the DCM. This vertical trend was also confirmed by the cytometry standardized fluorescence for the picoplankton community. Third, in both cruises, c_p* (660) varied through the water column following expected changes in intracellular pigmentation resulting from photoacclimation to the vertical light gradient, as previously observed in several works (e.g., Fennel and Boss, 2003; Mignot et al., 2014; Mitchell and Kiefer, 1988). Overall, these observations indicate that during the SUMMER cruises phytoplankton either dominate the c_p (660) signal or contributes a rather constant fraction covarying with the remaining pool of particles.

4.2. Phytoplankton pigments, community composition and size structure

The structure of phytoplankton assemblage observed during SUMMER cruises could be ascribed to the late-summer stratification (Sept-2011) and post-bloom (May-2012) periods of the phytoplankton seasonal cycle (Estrada et al., 2014; Latasa et al., 2010). In the NWMS, except for specific bloom events when the diatom-derived *Fuco* is dominant, the generally most abundant carotenoid irrespective of depth and time is *19'-HF* (Latasa et al., 2010; Marty et al., 2002; Siokou-Frangou et al., 2010), indicating that prymnesiophytes are the dominant group of phytoplankton. This, in turn, is in consonance with Royer et al. (2016), who found extremely high ratio of $DMSP_t$ (the algal osmolyte dimethylsulphoniopropionate) per unit of *Chl a* in both SUMMER cruises (with higher values in May-2012 than in Sept-2011), indicating the dominance of high DMSP producers, such as prymnesiophytes.

In the Mediterranean Sea, prymnesiophytes frequently coexist with picoprokaryotes and picoeukaryotes or alternate with dinoflagellates and other flagellates belonging to different algal groups (Estrada et al., 2014; Latasa et al., 2010). As reported here, higher abundance of *Synechococcus* and *Prochlorococcus* were observed in the Mediterranean Sea during the stably stratified period, thought the prokaryotic contribution was smaller during post-bloom conditions (Latasa et al., 2010; Marty and Chiaverini, 2002; Vidussi et al., 2000).

611 The phytoplankton community size structure, estimated using the DPA approach, evidenced
612 waters mostly codominated by picophytoplankton and nanophytoplankton in Sept-2011 and by
613 nanophytoplankton in May-2012. Accordingly, the size index (*SI*) showed lower values at the Middle
614 and DCM layers of Sept-2011 than May-2012, though both cruises presented a narrow range of
615 variation in this metric. Our observations of differences in the community size structure between
616 September and May were similar to that reported by Mayot et al. (2017) in the NWMS
617 (DYFAMED/BOUSSOLE site), using DPA derived biomass fractions. It must be noted that we made
618 strong assumptions when applying the DPA analysis (see Brewin et al., 2014, and references
619 therein). For example, a given diagnostic pigment could be shared by different size classes or some
620 taxonomic groups that harbour specific diagnostic pigments may vary in size. Besides and as
621 aforementioned, the *SI* index was originally developed for the surface layer and can be used here
622 only as a rough indicator of the phytoplankton dominant size in the three evaluated layers. Even
623 though, it has been previously used in different studies either in the SML or below this layer
624 (Kheireddine et al., 2018; Organelli et al., 2011; Wang et al., 2014). Is encouraging, however, the
625 agreement between our observations (DPA, light microscopy counts and cytometry determinations),
626 as well as with the previously mentioned works and other studies conducted in the NWMS (see
627 Bricaud et al., 2004; Organelli et al., 2013). This suggests that DPA provides here a realistic
628 description of the "bulk size structure" of the phytoplankton assemblages.

629 **4.3. Comparing the impacts of photoacclimation and phytoplankton community size**
630 **structure on phytoplankton absorption**

631 The analysis of the chlorophyll-specific absorption coefficient, a^*_{ph} (440), showed remarkable
632 vertical and inter-cruise differences. Several studies in the last three decades have tried to quantify
633 the intermingled effects of pigment packaging and pigment composition on a^*_{ph} (440) (e.g., Bricaud
634 and Stramski, 1990; Ferreira et al., 2013; Lutz et al., 1996; Morel, 1978). In these studies, much of
635 the observed variability was explained by the interplay between short-term cellular acclimation to
636 the prevailing growth conditions and the species composition of phytoplankton community. The
637 comprehensive examination presented here indicates that around 50% of the vertical variability of
638 a^*_{ph} (440) was explained by changes in the pigment composition with depth (ruled by the
639 photoprotective pigments) as a result of photoacclimation to the vertical light gradient. This
640 observation coincides with previous studies (Allali et al., 1997; Bouman et al., 2000; Letelier et al.,
641 2017), indicating that, if we aim to constrain estimates of pelagic primary production, we need to
642 improve our knowledge of how environmental factors affect the pigment composition of
643 phytoplankton assemblages and how much of the light absorbed by phytoplankton actually
644 translates into photosynthetic activity.

645 Changes in pigment composition, however, do not explain the observed vertical decrease in
646 the photosynthetic fraction of phytoplankton absorption nor the inter-cruise differences of a^*_{ph} (440)
647 in the SUMMER cruises. These were associated with the packaging effect, as observed for the
648 spatial and temporal variation in the packaging index [$Q_a^*(440)$], that accounted for a substantial
649 amount of the a^*_{ph} (440) variability. The novelty of our analysis was the attempt to partition the
650 packaging effect to evaluate the interactive effects of the two intrinsic factors affecting them. Pigment

packaging is a positive function of both cell size and intracellular concentration of pigments and an increase of either of these two terms will result in a corresponding decrease in $a^*_{ph}(\lambda)$ (Kirk, 1976; Morel and Bricaud, 1981). In natural waters, these terms can vary differently with the environmental factors (i.e., light history, nutrients, and temperature) and the phytoplankton community structure (e.g., Bricaud and Stramski, 1990; Ciotti et al., 2002; Stæhr et al., 2002). The overall effect on the packaging effect, and its consequences on the variability of $a^*_{ph}(440)$ (not explained by changes in pigment composition), will depend on the relative contributions of cell size and intracellular pigment concentration, and how they interact with each other.

In the SUMMER cruises, our main finding was to observe that differences in the $c_p^*(660)$ index, and therefore changes in photoacclimation, mainly explained the spatiotemporal variation in the packaging effect. On the other hand, our observations are not fully consistent with the general expectation that in natural waters changes in the packaging effect are mostly related to differences in cell size (e.g., Bricaud et al., 2004; Ciotti et al., 2002; Ferreira et al., 2013). Several of these studies, however, spanned a wide range of phytoplankton cell sizes and were carried out in surface waters of different oceanic areas, with a constrained impact of photoacclimation. Even under these conditions, a significant variation of the packing effect can be observed for a given value of *SI* (see Bricaud et al., 2004, their figure 8). Authors attributed part of this variation to different photoacclimation states. Therefore, is not surprising that at local scales photoacclimation can rule the packaging effect, especially when analyzing the entire euphotic zone and there are no major changes in the phytoplankton community structure.

Our observations are in line with different bio-optical studies that showed the significant contribution of photoacclimation to phytoplankton absorption dynamics and how cell size and intracellular pigment concentration can impact the packaging effect in different directions. For instance, Organelli et al. (2011) found, in a study conducted in autumn 2006, 2007 and 2008 for the upper and deeper euphotic layer, that the surface waters of the more oligotrophic areas of the Mediterranean Sea were characterized by larger cells with lower pigment packaging than those below the SML. Authors attributed this observation to vertical changes in cellular pigment concentrations. Furthermore, in a study conducted in the SML of the Black Sea during different seasons between 2011-2015, Churilova et al. (2017) showed a higher intracellular *Chl a* concentration and lower values of $a^*_{ph}(\lambda)$ in winter, in response to the 10-fold lower daily irradiance than that registered in summer, despite the dominance of large diatoms. Also in the Black Sea, Churilova et al. (2019) reported in a study conducted during periods of seasonal stratification between 1996-2016, a little variation of $a^*_{ph}(678)$ through the euphotic zone, due to the opposite impact of the increase in the intracellular pigment concentration with depth and the decrease of cell size. Moreover, during a cruise across the Atlantic Ocean between 21 October and 21 November 2014, Nunes et al. (2019) found that values of $a^*_{ph}(443)$ in the surface layer were uncorrelated with indicators of the phytoplankton size structure and were mainly explained by differences in pigment composition and the packaging effect due to changes in the intracellular pigment concentration.

5.0 CONCLUSIONS

In the presented analysis, we were able to use a suite of optical and biological parameters to explicitly separate the contribution of changes in pigment composition and pigment packaging on $a^*_{ph}(440)$ variability. Further, we partitioned the packaging effect into its two intrinsic terms (cell size and intracellular pigment composition). Our observations indicate that the variability of $a^*_{ph}(440)$ was mainly determined by photoacclimation to the vertical light gradient and the seasonal changes in light exposure.

Changes in the intracellular pigment concentration with depth increased the vertical effect of the photoprotective carotenoids and explained the differences between cruises in the phytoplankton chlorophyll-specific absorption. Our findings emphasize the need for increased efforts to investigate the impact of photoacclimation on $a^*_{ph}(\lambda)$ variability with implications on the correct evaluation of the packaging effect, thus constraining the natural variability of phytoplankton absorption unexplained by changes in the community size structure. This requires bio-optical studies that include a detailed analysis of the phytoplankton community size structure in the euphotic zone using different approaches (e.g., DPA, size-fractionated filtration and cells counts) coupled with robust indices of photoacclimation. This, in turn, should improve our comprehension of deviations of bio-optical models that contemplate the variability of phytoplankton absorption.

Acknowledgments

The authors acknowledge the invaluable assistance and cooperation of the marine technicians (UTM) and the crew aboard R/V Garcia del Cid. This research was funded by the successive Spanish Ministries of Science through projects SUMMER “SUrface Mixing Modulation of the Exposure to solar Radiation” (CTM2008– 03309/MAR), BIOGAPS (CTM2016-81008-R) and DOREMI (CTM2012– 34294), and through the CONICET and CONICET-CSIC scholarships to G. L. Pérez. This is a contribution of the Research Group on Marine Biogeochemistry and Global Change and that of Microbial Diversity and Function in Aquatic Environments, funded by the Catalan Government.

References

Allali, K., Bricaud, A., Claustre, H., 1997. Spatial variations in the chlorophyll-specific absorption coefficients of phytoplankton and photosynthetically active pigments in the equatorial Pacific. J. Geophys. Res. Ocean. 102, 12413–12423. https://doi.org/10.1029/97JC00380

Babin, M., Morel, A., Claustre, H., Bricaud, A., Kolber, Z., Falkowski, P.G., 1996. Nitrogen- and irradiance-dependent variations of the maximum quantum yield of carbon fixation in eutrophic, mesotrophic and oligotrophic marine systems. Deep Sea Res. Part I Oceanogr. Res. Pap. 43, 1241–1272. https://doi.org/10.1016/0967-0637(96)00058-1

Baker, K.S., Frouin, R., 1987. Relation between photosynthetically available radiation and total insolation at the ocean surface under clear skies1. Limnol. Oceanogr. 32, 1370–1377. https://doi.org/10.4319/lo.1987.32.6.1370

730 Barbieux, M., Uitz, J., Gentili, B., de Fommervault, O., Mignot, A., Poteau, A., Schmechtig, C.,
731 Taillandier, V., Leymarie, E., Penkerc'h, C., D'Ortenzio, F., Claustre, H., Bricaud, A., 2019. Bio-
732 optical characterization of subsurface chlorophyll maxima in the Mediterranean Sea from a
733 Biogeochemical-Argo float database. Biogeosciences 16, 1321–1342.
734 https://doi.org/10.5194/bg-16-1321-2019

735 Behrenfeld, M.J., Falkowski, P.G., 1997. A consumer's guide to phytoplankton primary productivity
736 models. Limnol. Oceanogr. 42, 1479–1491. https://doi.org/10.4319/lo.1997.42.7.1479

737 Behrenfeld, M.J., Boss, E., 2003. The beam attenuation to chlorophyll ratio: an optical index of
738 phytoplankton physiology in the surface ocean? Deep Sea Res. Part I Oceanogr. Res. Pap. 50,
739 1537–1549. https://doi.org/https://doi.org/10.1016/j.dsr.2003.09.002

740 Behrenfeld, M.J., Boss, E., 2006. Beam attenuation and chlorophyll concentration as alternative
741 optical indices of phytoplankton biomass. J. Mar. Res. 64, 431–451.
742 https://doi.org/10.1357/002224006778189563

743 Bidigare, R.R., Ondrusek, M.E., Morrow, J.H., Kiefer, D.A., 1990. In-vivo absorption properties of
744 algal pigments, in: Proc. SPIE 1302, Ocean Optics X, 290–302.
745 https://doi.org/10.1117/12.21451

746 Boss, E., Twardowski, M.S., Herring, S., 2001. Shape of the particulate beam attenuation
747 spectrum and its inversion to obtainthe shape of the particulate size distribution. Appl. Opt. 40,
748 4885–4893. https://doi.org/10.1364/AO.40.004885

749 Bouman, H.A., Platt, T., Kraay, G.W., Sathyendranath, S., Irwin, B.D., 2000. Bio-optical properties
750 of the subtropical North Atlantic. I. Vertical variability. Mar. Ecol. Prog. Ser. 200, 3–18.

751 Brewin, R.J.W., Hardman-Mountford, N.J., Lavender, S.J., Raitsos, D.E., Hirata, T., Uitz, J.,
752 Devred, E., Bricaud, A., Ciotti, Á.M., Gentili, B., 2011. An intercomparison of bio-optical
753 techniques for detecting dominant phytoplankton size class from satellite remote sensing.
754 Remote Sens. Environ. 115, 325–339. https://doi.org/https://doi.org/10.1016/j.rse.2010.09.004

755 Brewin, R.J.W., Sathyendranath, S., Lange, P.K., Tilstone, G., 2014. Comparison of two methods
756 to derive the size-structure of natural populations of phytoplankton. Deep Sea Res. Part I
757 Oceanogr. Res. Pap. 85, 72–79. https://doi.org/https://doi.org/10.1016/j.dsr.2013.11.007

758 Bricaud, A., Allali, K., Morel, A., Marie, D., Veldhuis, M. J., Partensky, F., Vaulot, D., 1999. Divinyl
759 chlorophyll a-specific absorption coefficients and absorption efficiency factors for
760 Prochlorococcus marinus: kinetics of photoacclimation. Mar. Ecol. Prog. Ser. 188, 21-32.

761 Bricaud, A., Babin, M., Claustre, H., Ras, J., Tièche, F., 2010. Light absorption properties and
762 absorption budget of Southeast Pacific waters. J. Geophys. Res. Ocean. 115, C08009.
763 https://doi.org/10.1029/2009JC005517

764 Bricaud, A., Babin, M., Morel, A., Claustre, H., 1995. Variability in the chlorophyll-specific
765 absorption coefficients of natural phytoplankton: Analysis and parameterization. J. Geophys.
766 Res. Ocean. 100, 13321–13332. https://doi.org/10.1029/95JC00463

Bricaud, A., Ciotti, Á.M., Gentili, B., 2012. Spatial-temporal variations in phytoplankton size and colored detrital matter absorption at global and regional scales, as derived from twelve years of SeaWiFS data (1998-2009). Global Biogeochem. Cycles 26, GB1010. https://doi.org/10.1029/2010GB003952

Bricaud, A., Claustre, H., Ras, J., Oubelkheir, K., 2004. Natural variability of phytoplanktonic absorption in oceanic waters: Influence of the size structure of algal populations. J. Geophys. Res. Ocean. 109, C11010. https://doi.org/10.1029/2004JC002419

Bricaud, A., Morel, A., Babin, M., Allali, K., Claustre, H., 1998. Variations of light absorption by suspended particles with chlorophyll a concentration in oceanic (case 1) waters: Analysis and implications for bio-optical models. J. Geophys. Res. Ocean. 103, 31033–31044. https://doi.org/10.1029/98JC02712

Bricaud, A., Stramski, D., 1990. Spectral absorption coefficients of living phytoplankton and nonalgal biogenous matter: A comparison between the Peru upwelling area and the Sargasso Sea. Limnol. Oceanogr. 35, 562–582. https://doi.org/10.4319/lo.1990.35.3.0562

Brunelle, C.B., Larouche, P., Gosselin, M., 2012. Variability of phytoplankton light absorption in Canadian Arctic seas. J. Geophys. Res. Ocean. 117, C00G17. https://doi.org/10.1029/2011JC007345

Campbell, L., Vaulot, D., 1993. Photosynthetic picoplankton community structure in the subtropical North Pacific Ocean near Hawaii (station ALOHA). Deep Sea Res. Part I Oceanogr. Res. Pap. 40, 2043–2060. https://doi.org/10.1016/0967-0637(93)90044-4

Chang, G.C., Dickey, T.D., 2004. Coastal ocean optical influences on solar transmission and radiant heating rate. J. Geophys. Res. Ocean. 109, C01020. https://doi.org/10.1029/2003JC001821

Churilova, T., Suslin, V., Krivenko, O., Efimova, T., Moiseeva, N., Mukhanov, V., Smirnova, L., 2017. Light absorption by phytoplankton in the upper mixed layer of the Black Sea: Seasonality and parametrization. Front. Mar. Sci. 4, 90. https://doi.org/10.3389/fmars.2017.00090

Churilova, T., Suslin, V., Sosik, H.M., Efimova, T., Moiseeva, N., Moncheva, S., Mukhanov, V., Rylkova, O., Krivenko, O., 2019. Phytoplankton light absorption in the deep chlorophyll maximum layer of the Black Sea. Eur. J. Remote Sens. 52, 123–136. https://doi.org/10.1080/22797254.2018.1533389

Ciotti, Á.M., Lewis, M.R., Cullen, J.J., 2002. Assessment of the relationships between dominant cell size in natural phytoplankton communities and the spectral shape of the absorption coefficient. Limnol. Oceanogr. 47, 404–417. https://doi.org/10.4319/lo.2002.47.2.0404

Cleveland, J.S., 1995. Regional models for phytoplankton absorption as a function of chlorophyll a concentration. J. Geophys. Res. Ocean. 100, 13333–13344. https://doi.org/10.1029/95jc00532

802 Cleveland, J.S., Weidemann, A.D., 1993. Quantifying absorption by aquatic particles: A multiple
803 scattering correction for glass-fiber filters. Limnol. Oceanogr. 38, 1321–1327.
804 https://doi.org/10.4319/lo.1993.38.6.1321

805 Cullen, J.J., 2015. Subsurface chlorophyll maximum layers: enduring enigma or mystery solved?
806 Ann. Rev. Mar. Sci. 7, 207–239. https://doi.org/10.1146/annurev-marine-010213-135111

807 D'Ortenzio, F., Iudicone, D., de Boyer Montegut, C., Testor, P., Antoine, D., Marullo, S., Santoleri,
808 R., Madec, G., 2005. Seasonal variability of the mixed layer depth in the Mediterranean Sea as
809 derived from in situ profiles. Geophys. Res. Lett. 32, L12605.
810 https://doi.org/10.1029/2005GL022463

811 D'Ortenzio, F., Marullo, S., Ragni, M., Ribera d'Alcalà, M., Santoleri, R., 2002. Validation of
812 empirical SeaWiFS algorithms for chlorophyll-a retrieval in the Mediterranean Sea: A case
813 study for oligotrophic seas. Remote Sens. Environ. 82, 79–94.
814 https://doi.org/https://doi.org/10.1016/S0034-4257(02)00026-3

815 Dall'Olmo, G., Westberry, T.K., Behrenfeld, M.J., Boss, E., Slade, W.H., 2009. Significant
816 contribution of large particles to optical backscattering in the open ocean. Biogeosciences 6,
817 947–967. https://doi.org/10.5194/bg-6-947-2009

818 de Boyer Montégut, C., Madec, G., Fischer, A.S., Lazar, A., Iudicone, D., 2004. Mixed layer depth
819 over the global ocean: An examination of profile data and a profile-based climatology. J.
820 Geophys. Res. Ocean. 109, C12003. https://doi.org/10.1029/2004JC002378

821 Estrada, M., Latasa, M., Emelianov, M., Gutiérrez-Rodríguez, A., Fernández-Castro, B., Isern-
822 Fontanet, J., Mouriño-Carballido, B., Salat, J., Vidal, M., 2014. Seasonal and mesoscale
823 variability of primary production in the deep winter-mixing region of the NW Mediterranean.
824 Deep Sea Res. Part I Oceanogr. Res. Pap. 94, 45–61.
825 https://doi.org/https://doi.org/10.1016/j.dsr.2014.08.003

826 Fennel, K., Boss, E., 2003. Subsurface maxima of phytoplankton and chlorophyll: Steady-state
827 solutions from a simple model. Limnol. Oceanogr. 48, 1521–1534.
828 https://doi.org/10.4319/lo.2003.48.4.1521

829 Ferreira, A., Ciotti, Á.M., Mendes, C.R.B., Uitz, J., Bricaud, A., 2017. Phytoplankton light
830 absorption and the package effect in relation to photosynthetic and photoprotective pigments in
831 the northern tip of Antarctic Peninsula. J. Geophys. Res. Ocean. 122, 7344–7363.
832 https://doi.org/10.1002/2017JC012964

833 Ferreira, A., Garcia, V.M.T., Garcia, C.A.E., 2009. Light absorption by phytoplankton, non-algal
834 particles and dissolved organic matter at the Patagonia shelf-break in spring and summer.
835 Deep Sea Res. Part I Oceanogr. Res. Pap. 56, 2162–2174.
836 https://doi.org/10.1016/j.dsr.2009.08.002

837 Ferreira, A., Stramski, D., Garcia, C.A.E., Garcia, V.M.T., Ciotti, Á.M., Mendes, C.R.B., 2013.
838 Variability in light absorption and scattering of phytoplankton in Patagonian waters: Role of

community size structure and pigment composition. J. Geophys. Res. Ocean. 118, 698–714. https://doi.org/10.1002/jgrc.20082

Fujiki, T., Taguchi, S., 2002. Variability in chlorophyll a specific absorption coefficient in marine phytoplankton as a function of cell size and irradiance. J. Plankton Res. 24, 859–874. https://doi.org/10.1093/plankt/24.9.859

Gasol, J.M., Del Giorgio, P.A., 2000. Using flow cytometry for counting natural planktonic bacteria and understanding the structure of planktonic bacterial communities. Sci. Mar. 64, 197–224. https://doi.org/10.3989/scimar.2000.64n2197

Gasol J.M., Morán X.A.G., 2015. Flow Cytometric Determination of Microbial Abundances and Its Use to Obtain Indices of Community Structure and Relative Activity, In: McGenity T., Timmis K., Nogales B. (Eds.), Hydrocarbon and Lipid Microbiology Protocols. Springer Protocols Handbooks. Springer, Berlin, pp. 159-187. https://doi.org/10.1007/8623_2015_139

Gernez, P., Antoine, D., Huot, Y., 2011. Diel cycles of the particulate beam attenuation coefficient under varying trophic conditions in the northwestern Mediterranean Sea: Observations and modeling. Limnol. Oceanogr. 56, 17–36. https://doi.org/10.4319/lo.2011.56.1.0017

Goericke, R., Repeta, D., 1993. Chlorophylls a and b and divinyl chlorophylls a and b in the open subtropical North Atlantic Ocean. Mar. Ecol. Prog. Ser. 101, 307–313. https://doi.org/10.3354/meps101307

Hargreaves, B.R., Girdner, S.F., Buktenica, M.W., Collier, R.W., Urbach, E., Larson, G.L., 2007. Ultraviolet radiation and bio-optics in Crater Lake, Oregon. Hydrobiologia 574, 107–140. https://doi.org/10.1007/s10750-006-0348-0

Hickman, A.E., Holligan, P.M., Moore, C.M., Sharples, J., Krivtsov, V., Palmer, M.R., 2009. Distribution and chromatic adaptation of phytoplankton within a shelf sea thermocline. Limnol. Oceanogr. 54, 525–536. https://doi.org/10.4319/lo.2009.54.2.0525

IOCCG Protocol Series, 2018. Inherent Optical Property Measurements and Protocols: Absorption Coefficient, Neeley, A. R. and Mannino, A. (Eds.), IOCCG Ocean Optics and Biogeochemistry Protocols for Satellite Ocean Colour Sensor Validation, Volume 1.0, IOCCG, Dartmouth, NS, Canada.

Johnsen, G., Bricaud, A., Nelson, N., Prézelin, B.B., Bidigare, R.R., 2011. In vivo bio-optical properties of phytoplankton pigments, in: Roy, S., Llewellyn, C., Egeland, E. S., Johnsen, G. (Eds.), Phytoplankton Pigments: Characterization, Chemotaxonomy and Applications in Oceanography. Cambridge University Press, Cambridge, pp. 496–537.

Kheireddine, M., Ouhssain, M., Organelli, E., Bricaud, A., Jones, B.H., 2018. Light absorption by suspended particles in the Red Sea: Effect of phytoplankton community size structure and pigment composition. J. Geophys. Res. Ocean. 123, 902–921. https://doi.org/10.1002/2017JC013279

875 Kirk, J. T. O., 2011. Light and Photosynthesis in Aquatic Ecosystems, third ed. Cambridge
876 University Press, Cambridge.

877 Kirk, J.T.O., 1976. A theoretical analysis of the contribution of algal cells to the attenuation of light
878 within natural waters. New Phytol. 77, 341–358. https://doi.org/10.1111/j.1469-
879 8137.1976.tb01524.x

880 Kishino, M., N. Takahashi, N. Okami, and S. Ichimura. 1985. Estimation of the spectral absorption
881 coefficients of phytoplankton in the sea. Bull. Mar. Sci. 37, 634-642.

882 Latasa, M., Scharek, R., Vidal, M., Vila-Reixach, G., Gutiérrez-Rodríguez, A., Emelianov, M.,
883 Gasol, J., 2010. Preferences of phytoplankton groups for waters of different trophic status in
884 the northwestern Mediterranean Sea. Mar. Ecol. Prog. Ser. 407, 27–42.
885 https://doi.org/10.3354/meps08559

886 Lavigne, H., D'Ortenzio, F., Ribera D'Alcalà, M., Claustre, H., Sauzède, R., Gacic, M., 2015. On
887 the vertical distribution of the chlorophyll a concentration in the Mediterranean Sea: a basin-
888 scale and seasonal approach. Biogeosciences 12, 5021–5039. https://doi.org/10.5194/bg-12-
889 5021-2015

890 Lazzara, L., Bricaud, A., Claustre, H., 1996. Spectral absorption and fluorescence excitation
891 properties of phytoplanktonic populations at a mesotrophic and an oligotrophic site in the
892 tropical North Atlantic (EUMELI program). Deep Sea Res. Part I Oceanogr. Res. Pap. 43,
893 1215–1240. https://doi.org/10.1016/0967-0637(96)00057-X

894 Lee, Z., Marra, J., Perry, M.J., Kahru, M., 2015. Estimating oceanic primary productivity from
895 ocean color remote sensing: A strategic assessment. J. Mar. Syst. 149, 50–59.
896 https://doi.org/10.1016/j.jmarsys.2014.11.015

897 Lefort, T., Gasol, J.M., 2014. Short-time scale coupling of picoplankton community structure and
898 single-cell heterotrophic activity in winter in coastal NW Mediterranean Sea waters. J. Plankton
899 Res. 36, 243–258. https://doi.org/10.1093/plankt/fbt073

900 Letelier, R.M., Karl, D.M., Abbott, M.R., Bidigare, R.R., 2004. Light driven seasonal patterns of
901 chlorophyll and nitrate in the lower euphotic zone of the North Pacific Subtropical Gyre. Limnol.
902 Oceanogr. 49, 508–519. https://doi.org/10.4319/lo.2004.49.2.0508

903 Letelier, R.M., White, A.E., Bidigare, R.R., Barone, B., Church, M.J., Karl, D.M., 2017. Light
904 absorption by phytoplankton in the North Pacific Subtropical Gyre. Limnol. Oceanogr. 62,
905 1526–1540. https://doi.org/10.1002/lno.10515

906 Lohrenz, S.E., Weidemann, A.D., Tuel, M., 2003. Phytoplankton spectral absorption as influenced
907 by community size structure and pigment composition. J. Plankton Res. 25, 35–61.
908 https://doi.org/10.1093/plankt/25.1.35

909 Loisel, H., Morel, A., 1998. Light scattering and chlorophyll concentration in case 1 waters: A
910 reexamination. Limnol. Oceanogr. 43, 847–858. https://doi.org/10.4319/lo.1998.43.5.0847

Loisel, H., Vantrepotte, V., Norkvist, K., Mériaux, X., Kheireddine, M., Ras, J., Pujo-Pay, M., Combet, Y., Leblanc, K., Dall'Olmo, G., Mauriac, R., Dessailly, D., Moutin, T., 2011. Characterization of the bio-optical anomaly and diurnal variability of particulate matter, as seen from scattering and backscattering coefficients, in ultra-oligotrophic eddies of the Mediterranean Sea. Biogeosciences 8, 3295–3317. https://doi.org/10.5194/bg-8-3295-2011

Lutz, V.A, Sathyendranath, S., Head, E.J.H., 1996. Absorption coefficient of phytoplankton: regional variations in the North Atlantic. Mar. Ecol. Prog. Ser. 135, 197–213. https://doi.org/10.3354/meps135197

Marra, J., Trees, C.C., O'Reilly, J.E., 2007. Phytoplankton pigment absorption: A strong predictor of primary productivity in the surface ocean. Deep Sea Res. Part I Oceanogr. Res. Pap. 54, 155–163. https://doi.org/10.1016/j.dsr.2006.12.001

Marty, J.-C., Chiavérini, J., 2002. Seasonal and interannual variations in phytoplankton production at DYFAMED time-series station, northwestern Mediterranean Sea. Deep Sea Res. Part II Top. Stud. Oceanogr. 49, 2017–2030. https://doi.org/10.1016/S0967-0645(02)00025-5

Marty, J.-C., Chiavérini, J., Pizay, M.-D., Avril, B., 2002. Seasonal and interannual dynamics of nutrients and phytoplankton pigments in the western Mediterranean Sea at the DYFAMED time-series station (1991–1999). Deep Sea Res. Part II Top. Stud. Oceanogr. 49, 1965–1985. https://doi.org/10.1016/S0967-0645(02)00022-X

Mayot, N., D'Ortenzio, F., Uitz, J., Gentili, B., Ras, J., Vellucci, V., Golbol, M., Antoine, D., Claustre, H., 2017. Influence of the phytoplankton community structure on the spring and annual primary production in the Northwestern Mediterranean Sea. J. Geophys. Res. Ocean. 122, 9918–9936. https://doi.org/10.1002/2016JC012668

Mignot, A., Claustre, H., Uitz, J., Poteau, A., D'Ortenzio, F., Xing, X., 2014. Understanding the seasonal dynamics of phytoplankton biomass and the deep chlorophyll maximum in oligotrophic environments: A Bio-Argo float investigation. Global Biogeochem. Cycles. 28, 856–876. https://doi.org/10.1002/2013GB004781

Mitchell, B. G., 1990. Algorithms for determining the absorption coefficient for aquatic particulates using the quantitative filter technique. In: Proc.SPIE, 1302, Ocean Optics X, 137–148. https://doi.org/10.1117/12.21440

Mitchell, B., Holm-Hansen, O., 1991. Bio-optical properties of Antarctic Peninsula waters: differentiation from temperate ocean models. Deep Sea Res. Part A. Oceanogr. Res. Pap. 38, 1009–1028. https://doi.org/10.1016/0198-0149(91)90094-V

Mitchell, B.G., Kiefer, D.A., 1988. Chlorophyll α specific absorption and fluorescence excitation spectra for light-limited phytoplankton. Deep Sea Res. Part A. Oceanogr. Res. Pap. 35, 639–663. https://doi.org/10.1016/0198-0149(88)90024-6

Moore, L.R., Goericke, R., Chisholm, S.W., 1995. Comparative physiology of Synechococcus and Prochlorococcus: influence of light and temperature on growth, pigments, fluorescence and absorptive properties. Mar. Ecol. Prog. Ser. 116, 259–275.

6611(91)90004-6

Morel, A., 1978. Available, usable, and stored radiant energy in relation to marine photosynthesis. Deep Sea Res. 25, 673–688. https://doi.org/10.1016/0146-6291(78)90623-9

Morel, A., 1991. Light and marine photosynthesis: a spectral model with geochemical and climatological implications. Prog. Ocean. 26, 263–306. https://doi.org/10.1016/0079-

Morel, A., Ahn, Y.H., Partensky, F., Vaulot, D., Claustre, H., 1993. Prochlorococcus and Synechococcus: A comparative study of their optical properties in relation to their size and pigmentation. J. Mar. Res. 51, 617–649. https://doi.org/10.1357/0022240933223963

Morel, A., Antoine, D., Babin, M., Dandonneau, Y., 1996. Measured and modeled primary production in the northeast Atlantic (EUMELI JGOFS program): The impact of natural variations in photosynthetic parameters on model predictive skill. Deep Res Part I Oceanogr. Res. Pap. 43, 1273–1304. https://doi.org/10.1016/0967-0637(96)00059-3

Morel, A., Bricaud, A., 1981. Theoretical results concerning light absorption in a discrete medium, and application to specific absorption of phytoplankton. Deep Sea Res. Part A. Oceanogr. Res. Pap. 28, 1375–1393. https://doi.org/10.1016/0198-0149(81)90039-X

Morel, A., Maritorena, S., 2001. Bio-optical properties of oceanic waters: A reappraisal. J. Geophys. Res. Ocean. 106, 7163–7180. https://doi.org/10.1029/2000JC000319

Nunes, S., Pérez, G.L., Latasa, M., Zamanillo, M., Delgado, M., Ortega-Retuerta, E., Marrasé, C., Simó, R., Estrada, M., 2019. Size fractionation, chemotaxonomic groups and bio-optical properties of phytoplankton along a transect from the Mediterranean Sea to the SW Atlantic Ocean. Sci. Mar. 83, 87–109. http://dx.doi.org/10.3989/scimar.04866.10A

O'Reilly, J.E., Maritorena, S., Mitchell, B.G., Siegel, D.A., Carder, K.L., Garver, S.A., Kahru, M., McClain, C., 1998. Ocean color chlorophyll algorithms for SeaWiFS. J. Geophys. Res. Ocean. 103, 24937–24953. https://doi.org/10.1029/98JC02160

Organelli, E., Bricaud, A., Antoine, D., Uitz, J., 2013. Multivariate approach for the retrieval of phytoplankton size structure from measured light absorption spectra in the Mediterranean Sea (BOUSSOLE site). Appl. Opt. 52, 2257–2273. https://doi.org/10.1364/AO.52.002257

Organelli, E., Nuccio, C., Melillo, C., Massi, L., 2011. Relationships between phytoplankton light absorption, pigment composition and size structure in offshore areas of the Mediterranean Sea. Adv. Oceanogr. Limnol. 2, 107–123. https://doi.org/10.1080/19475721.2011.607489

Pasqueron de Fommervault, O., D'Ortenzio, F., Mangin, A., Serra, R., Migon, C., Claustre, H., Lavigne, H., Ribera d'Alcalà, M., Prieur, L., Taillandier, V., Schmechtig, C., Poteau, A., Leymarie, E., Dufour, A., Besson, F., Obolensky, G., 2015. Seasonal variability of nutrient concentrations in the Mediterranean Sea: Contribution of Bio-Argo floats. J. Geophys. Res. Ocean. 120, 8528–8550. https://doi.org/10.1002/2015JC011103

Preisendorfer, R.W., 1961. Application of radiative transfer theory to light measurements in the sea. Monographs 10. International Union of Geodesy and Geophysics, Paris, 11–30.

R Development Core Team, 2004. R: A Language And environment for Statistical Computing, R Found. for Stat. Comput.

Royer, S.-J., Galí, M., Mahajan, A.S., Ross, O.N., Pérez, G.L., Saltzman, E.S., Simó, R., 2016. A high-resolution time-depth view of dimethylsulphide cycling in the surface sea. Sci. Rep. 6, 32325. https://doi.org/10.1038/srep32325

Sathyendranath, S., Platt, T., 1988. The spectral irradiance field at the surface and in the interior of the ocean: A model for applications in oceanography and remote sensing. J. Geophys. Res. Ocean. 93, 9270–9280. https://doi.org/10.1029/JC093iC08p09270

Siegel, D.A., Behrenfeld, M.J., Maritorena, S., McClain, C.R., Antoine, D., Bailey, S.W., Bontempi, P.S., Boss, E.S., Dierssen, H.M., Doney, S.C., Eplee, R.E., Evans, R.H., Feldman, G.C., Fields, E., Franz, B.A., Kuring, N.A., Mengelt, C., Nelson, N.B., Patt, F.S., Robinson, W.D., Sarmiento, J.L., Swan, C.M., Werdell, P.J., Westberry, T.K., Wilding, J.G., Yoder, J.A., 2013. Regional to global assessments of phytoplankton dynamics from the SeaWiFS mission. Remote Sens. Environ. 135, 77–91. https://doi.org/10.1016/j.rse.2013.03.025

Siokou-Frangou, I., Christaki, U., Mazzocchi, M.G., Montresor, M., Ribera d'Alcalá, M., Vaqué, D., Zingone, A., 2010. Plankton in the open Mediterranean Sea: a review. Biogeosciences 7, 1543–1586. https://doi.org/10.5194/bg-7-1543-2010

Stæhr, P.A., Henriksen, P., Markager, S., 2002. Photoacclimation of four marine phytoplankton species to irradiance and nutrient availability. Mar. Ecol. Prog. Ser. 238, 47–59. https://doi.org/10.3354/meps238047

Stæhr, P.A., Markager, S., Sand-Jensen, K., 2004. Pigment specific in vivo light absorption of phytoplankton from estuarine, coastal and oceanic waters. Mar. Ecol. Prog. Ser. 275, 115–128. https://doi.org/10.3354/meps275115

Stramski, D., Kiefer, D.A., 1991. Light scattering by microorganisms in the open ocean. Prog. Oceanogr. 28, 343–383. https://doi.org/10.1016/0079-6611(91)90032-H

Stuart, V., Sathyendranath, S., Platt, T., Maass, H., Irwin, B.D., 1998. Pigments and species composition of natural phytoplankton populations: effect on the absorption spectra. J. Plankton Res. 20, 187–217. https://doi.org/10.1093/plankt/20.2.187

Tilstone, G.H., Taylor, B.H., Blondeau-Patissier, D., Powell, T., Groom, S.B., Rees, A.P., Lucas, M.I., 2015. Comparison of new and primary production models using SeaWiFS data in contrasting hydrographic zones of the northern North Atlantic. Remote Sens. Environ. 156, 473–489. https://doi.org/10.1016/j.rse.2014.10.013

Trüper, H. G., & Yentsch, C. S. (1967). Use of glass fiber filters for the rapid preparation of in vivo absorption spectra of photosynthetic bacteria. Journal of Bacteriology, 94, 1255– 1256.

Uitz, J., Claustre, H., Morel, A., Hooker, S.B., 2006. Vertical distribution of phytoplankton communities in open ocean: An assessment based on surface chlorophyll. J. Geophys. Res. Ocean. 111, C08005. https://doi.org/10.1029/2005JC003207

Uitz, J., Stramski, D., Reynolds, R.A., Dubranna, J., 2015. Assessing phytoplankton community composition from hyperspectral measurements of phytoplankton absorption coefficient and remote-sensing reflectance in open-ocean environments. Remote Sens. Environ. 171, 58–74. https://doi.org/10.1016/j.rse.2015.09.027

Utermöhl, H., 1958. Methods of collecting plankton for various purposes are discussed. SIL Commun. 1953-1996, 9, 1–38. https://doi.org/10.1080/05384680.1958.11904091

van Leeuwe, M.A., van Sikkelerus, B., Gieskes, W.W.C., Stefels, J., 2005. Taxon-specific differences in photoacclimation to fluctuating irradiance in an Antarctic diatom and a green flagellate. Mar. Ecol. Prog. Ser. 288, 9–19. https://doi.org/10.3354/meps288009

Vidussi, F., Claustre, H., Manca, B.B., Luchetta, A., Marty, J.-C., 2001. Phytoplankton pigment distribution in relation to upper thermocline circulation in the eastern Mediterranean Sea during winter. J. Geophys. Res. Ocean. 106, 19939–19956. https://doi.org/10.1029/1999JC000308.

Vidussi, F., Marty, J.-C., Chiavérini, J., 2000. Phytoplankton pigment variations during the transition from spring bloom to oligotrophy in the northwestern Mediterranean sea. Deep. Res. Part I Oceanogr. Res. Pap. 47, 423–445. https://doi.org/10.1016/S0967-0637(99)00097-7

Volpe, G., Santoleri, R., Vellucci, V., Ribera d'Alcalà, M., Marullo, S., D'Ortenzio, F., 2007. The colour of the Mediterranean Sea: Global versus regional bio-optical algorithms evaluation and implication for satellite chlorophyll estimates. Remote Sens. Environ. 107, 625–638. https://doi.org/10.1016/j.rse.2006.10.017

Wang, S.Q., Ishizaka, J., Yamaguchi, H., Tripathy, S.C., Hayashi, M., Xu, Y.J., Mino, Y., Matsuno, T., Watanabe, Y., Yoo, S.J., 2014. Influence of the Changjiang River on the light absorption properties of phytoplankton from the East China Sea. Biogeosciences 11, 1759–1773. https://doi.org/10.5194/bg-11-1759-2014

Westberry, T.K., Dall'Olmo, G., Boss, E., Behrenfeld, M.J., Moutin, T., 2010. Coherence of particulate beam attenuation and backscattering coefficients in diverse open ocean environments. Opt. Express 18, 15419–15425. https://doi.org/10.1364/OE.18.015419

Xing, X., Claustre, H., Blain, S., D'Ortenzio, F., Antoine, D., Ras, J., & Guinet, C. 2012. Quenching correction for in vivo chlorophyll fluorescence acquired by autonomous platforms: A case study with instrumented elephant seals in the Kerguelen region (Southern Ocean). Limnology and Oceanography: Methods 10, 483–495. https://doi.org/10.4319/lom.2012.10.483

Xing, X., Claustre, H., Uitz, J., Mignot, A., Poteau, A., Wang, H., 2014. Seasonal variations of bio-optical properties and their interrelationships observed by Bio-Argo floats in the subpolar North Atlantic. J. Geophys. Res. Ocean. 119, 7372–7388. https://doi.org/10.1002/2014JC010189

Zapata, M., Rodríguez, F., Garrido, J.L., 2000. Separation of chlorophylls and carotenoids from marine phytoplankton: a new HPLC method using a reversed phase C8 column and pyridine-containing mobile phases. Mar. Ecol. Prog. Ser. 195, 29–45.

Zeng, C., Rosengard, S.Z., Burt, W., Peña, M.A., Nemcek, N., Zeng, T., Arrigo, K.R., Tortell, P.D., 2018. Optically-derived estimates of phytoplankton size class and taxonomic group biomass in the Eastern Subarctic Pacific Ocean. Deep Sea Res. Part I Oceanogr. Res. Pap. 136, 107–118. https://doi.org/10.1016/j.dsr.2018.04.001

Declaration of Interest Statement

Declaration of interests

☒ The authors declare that they have no known competing financial interests or personal relationships that could have appeared to influence the work reported in this paper.

☐The authors declare the following financial interests/personal relationships which may be considered as potential competing interests: